Master's Thesis of Science
in Food Science and Biotechnology

Structure of flavoprotein RclA from food-borne pathogens, and its molecular mechanism contributing to hypochlorous acid resistance

식품 병원균 유래 플라빈단백질 RclA의 구조와 차아염소산 저항성에 기여하는 분자 기전

February 2020

Food Science and Biotechnology Major
Department of Agricultural Biotechnology
The Graduate School
Seoul National University

Yeongjin Baek

석사학위논문

Structure of flavoprotein RclA from food-borne pathogens, and its molecular mechanism contributing to hypochlorous acid resistance

지도교수 하 남 출

이 논문을 석사학위논문으로 제출함

2020년 2월

서울대학교 대학원

농생명공학부 식품생명공학전공

백 영 진

백영진의 석사학위논문을 인준함
2020년 2월

위원장	최 영 진	(인)
부위원장	하 남 출	(인)
위원	유 상 열	(인)

Abstract

Hypochlorous acid (HOCl) is a powerful sanitizer and has been used to control food-borne pathogens in various food sanitizing industries. The immune system generates HOCl to kill microorganisms via oxidative burst, and the toxicity of HOCl is amplified in the phagosome by importing Cu^{2+}. In *Escherichia coli* and *Salmonella*, the transcriptional regulator RclR recognizes HOCl stress and induces the RclA, B, and C proteins to defend against stress. However, the structure and biochemical roles of Rcl proteins remain to be elucidated. In this study, the role of the flavoprotein disulfide reductase (FDR) RclA in the survival of *Salmonella* in macrophage phagosomes was examined. To understand the molecular mechanism of RclA, the crystal structures of RclA from *E. coli* were determined. The homodimeric RclA was similar to typical FDRs, exhibiting two conserved cysteine residues near the flavin ring of the cofactor flavin adenine dinucleotide (FAD). Cu^{2+} accelerated the oxidation of NADH by RclA, leading to a lowering of the oxygen level in the solution. Cu^{2+} itself was reported to be reduced to become Cu^{+} during the NADH oxidation by RclA. Mutation of the conserved cysteine residues lowered the specificity to Cu^{2+} or substantially increased the production of superoxide anion in the absence of Cu^{2+} compared to the RclA wild type. The lowered oxygen level by RclA would contribute to the inhibition of oxidative bursts in phagosomes. The reduced Cu^{+} can be

exported by Cu^{+}-specific efflux pumps and would inhibit the toxic radical production by HOCl-Cu^{2+} reaction. This study provides the molecular basis of bacterial survival in HOCl stress from our immune systems. The HOCl resistance mechanism of RclA further gives an insight into controlling food-borne pathogens with HOCl-based sanitizers. Mimicking the phagosome environment by the combined treatment of HOCl with some inhibitors targeting RclA can lower the dose of HOCl treatment with the increased bactericidal effect.

Keywords: hypochlorous acid, flavoprotein disulfide reductase, copper, oxygen, crystal structure

Student Number: **2018-26723**

Contents

List of Figures

List of Table

I. Introduction

Hypochlorous acid (HOCl) is a well-known antibacterial agent, and it has been commonly used as a sanitizer in food industries to control food-borne pathogens (1-3). HOCl is also used in the innate immune systems of higher eukaryotes (4-6). To kill invading bacteria, macrophages and neutrophils in the immune system employ myeloperoxidase to generate HOCl from H_2O_2, which is produced by the oxidative burst from molecular oxygen by NADPH oxidase (7). HOCl directly oxidizes amino acids containing amines and sulfurs and can cleave DNA once it is converted into a deadly toxic hydroxyl radical in the presence of iron or copper ions via Fenton(-like) reaction (8-11).

HypT, RclR, and NemR are HOCl-responsive transcriptional factors in bacteria that increase bacterial survival under HOCl stress (12-14). HypT, belonging to the LysR-type transcriptional regulators, employs a HOCl-sensitive methionine residue to repress genes related to the import of iron to the cytosol in *Escherichia coli* and *Salmonella enterica* serovar Typhimurium. HypT plays a critical role in the survival of *Salmonella* in macrophages (15). NemR of *E. coli* is a redox-regulated transcriptional repressor that utilizes the oxidation status of HOCl-sensitive cysteine residues. NemR expresses two enzymes, GloA and NemA, to detoxify methylglyoxal and reactive electrophiles (14).

RclR is a member of the AraC family of transcriptional regulators

and senses HOCl with highly conserved cysteine residues (12,16). RclA, RclB, and RclC proteins were identified as RclR target genes in both *E. coli* and *Salmonella*. In *E. coli*, RclR, RclA, RclB, and RclC contribute to the HOCl-resistance of the bacterium. Deletion of any one of these genes decreases the survival of *E. coli* under HOCl stress (12). RclA putatively belongs to the flavoprotein disulfide reductase (FDR) family. RclB is a small uncharacterized periplasmic protein that has the signal sequence for secretion. RclC is a multipass inner membrane protein with homology to quinone-binding proteins. However, little is known about the biochemical functions of RclA, RclB, and RclC.

A recent study suggested that the FDR RclA is widely conserved among bacteria that colonize epithelial surfaces, and contributes to host colonization in environments with HOCl-mediated oxidative stress (17). FDRs usually form homodimers and use non-covalently bound flavin adenine dinucleotide (FAD) and a non-flavin redox center, catalyzing NAD(P)H-dependent reduction of a variety of substrates, such as sulfur-containing peptides, metal ions, H_2O_2, and O_2 (18). Like other FAD-dependent reductases, the reducing power of the bound FAD is supplied from the cytosolic NAD(P)H pool. FDRs can be divided into three subgroups depending on the non-flavin redox centers (18). Very recently, Derke *et al*. reported that RclA from *E. coli* exhibits Cu^{2+} reductase activity, reducing Cu^{2+} to Cu^{+} to cope with HOCl stress (17). Here, the crystal structures of RclA

from *E. coli* were determined, containing FAD at its active site. Based on the structures and the subsequent biochemical analyses, the functions of RclA in terms of HOCl resistance in bacteria were investigated.

The HOCl resistance mechanism of RclA gave insights into controlling food-borne pathogens with HOCl-based sanitizers in food processing. Inhibiting RclA of food-borne pathogens This work presents the combination method of HOCl with inhibitor inactivating RclA, to decrease the dose of HOCl and amplifying the bactericidal effect.

II. Experimental Procedures

2.1. Plasmid construction

To overexpress the full-length (1–441) RclA wild type, the gene encoding the protein was amplified by polymerase chain reaction (PCR) using the following two primers. The underlined sequences represent the EcoRI and HindIII restriction sites, respectively.

(Forward: 5'-GGCGAATTCATGAATAAATATCAGGCAG-3')

(Reverse: 5'- GCCAAGCTTTTATTTGACTAATGAAAATAG-3')

The amplified product and the expression vector pProEX-HTa (Invitrogen, USA) were digested with EcoRI and HindIII restriction enzymes. The digested PCR product was inserted into the digested expression vector pProEX-HTa by DNA ligase. The resulting plasmid encodes the hexahistidine tag and the TEV protease cleavage site at the N-terminus of the protein. The plasmids encoding RclA wild type protein were transformed into the *Escherichia coli* C43 (DE3) strain by the heat-shock method. The recombinant plasmid was confirmed by DNA sequencing.

2.2. Site-directed mutagenesis

To produce the RclA C43S and RclA C48S, a single mutation of cysteine to serine was performed using the Quick Change XL Site-directed Mutagenesis

Kit. The complementary mutagenic primers were designed using the QuikChange® Primer Design Program (19) and used to PCR reactions. After amplification, the PCR mixture was incubated with DpnI at 37℃ for 2 h. For overexpression of the recombinant DNA, each plasmid encoding RclA mutant was transformed into *E. coli* BL21 (DE3) competent cell by the heat-shock method. The sequence of the mutant plasmid was confirmed by DNA sequencing.

2.3. Purification of RclA wild type and mutants

2.3.1. Overexpression

For expression of the recombinant proteins, a single colony of *E. coli* C43 (DE3) and *E. coli* BL21 (DE3) was inoculated into 25 mL LB broth including 100 μg/mL ampicillin (Duchefa, Netherlands) and incubated at 37℃ for 14 h. Subsequently, the cells were cultured in 1.5 L Luria Broth medium containing 100 μg/mL ampicillin at 37°C until an OD_{600} of 0.7 was measured, and the protein expression was induced with 0.5 mM isopropyl-β-D-thiogalactopyranoside (IPTG) at 30°C for 6 h. The cells were harvested by centrifugation at 3850 g for 7 min. After harvest, cells were resuspended in lysis buffer containing 20 mM Tris-HCl (pH 8.0), 150 mM NaCl, and 2 mM 2-mercaptoethanol. The suspensions were disrupted using a continuous-type French press (Constant Systems Limited, United Kingdom) at 23 kpsi. The

crude lysate was centrifugated at 19,000 g for 30 min at 4°C and the pellet containing cell debris was discarded.

2.3.2. Affinity chromatography

The supernatant was loaded onto Ni^{2+}-NTA agarose resin (GE Healthcare) and rolled in a column for 45 min at 4°C. After washing the column with ~300 mL lysis buffer supplemented with 20 mM imidazole, the RclA wild-type protein was eluted with lysis buffer supplemented with 250 mM imidazole. The eluate was treated with recombinant TEV protease by incubation at room temperature for 12 h to cleave the hexahistidine tag.

2.3.3. Ion-exchange chromatography

The cleaved proteins were diluted four-fold with 20 mM Tris-HCl (pH 8.0) buffer containing 2 mM 2-mercaptoethanol and loaded onto a HiTrap Q column (GE Healthcare, USA). A linear gradient of increasing NaCl concentration was applied to the column. The eluted fractions containing the protein were pooled and concentrated.

2.3.4. Size exclusion chromatography (SEC) and concentration

The concentrated proteins were subjected to size-exclusion chromatography using a HiLoad 26/600 Superdex 200 pg column (GE Healthcare) equilibrated with 20 mM Tris-HCl (pH 8.0) buffer containing 150 mM NaCl and 2-

mercaptoethanol. The purified protein was concentrated up to 13 mg/mL using Vivaspin 20 (Sartorius, Germany) and stored at –80°C. Protein concentrations were determined based on FAD content using a previously determined ε_{456} of 11.3 mM^{-1} cm^{-1}.

2.4. Crystallization of RclA wild type and C43S

RclA proteins (wild type, C43S) were crystallized at 16°C using the hanging drop vapor diffusion method after mixing 1 µL protein solution and 1 µL precipitation solution. The RclA wild-type protein was first crystallized in a precipitation solution containing 0.2 M ammonium sulfate, 0.1 M Bis-Tris HCl (pH 5.8), 25% (w/v) PEG 3350, and 2 mM TCEP. Subsequently, the crystals were disrupted for microseeding and diluted with precipitation solution containing 0.2 M ammonium sulfate, 0.1 M Bis-Tris HCl (pH 5.8), 13% (w/v) PEG 3350, and 2 mM TCEP. Microseeding was performed by mixing 1 µL protein and 1 µL microseeds diluted with precipitation solution. The RclA wild-type crystals were briefly incubated in precipitation solution supplemented with 20% (v/v) glycerol as a cryoprotectant, and flash-frozen in liquid ethane at –88.5°C, and subsequently transferred into liquid nitrogen to collect the dataset. For the Cu^{2+}-soaked RclA wild-type structure, the crystals were incubated in a reservoir solution supplemented with 5 mM $CuCl_2$ for 15 h. The crystals were incubated in precipitation solution supplemented with 30% (v/v) glycerol and 5 mM $CuCl_2$ for 6 min, and flash-

frozen in liquid nitrogen to collect the dataset. RclA C43S was crystallized in a solution containing 0.05 mM ammonium sulfate, 0.05 mM Bis-Tris HCl (pH 5.8), and 30% pentaerythritol ethoxylate (15/4_EO/OH). Microseeding was performed using disrupted RclA C43S crystals, and was diluted with 0.05 mM ammonium sulfate, 0.05 mM Bis-Tris HCl (pH 5.8), 25% pentaerythritol ethoxylate (15/4_EO/OH). For Cu^{2+}-soaked RclA C43S structure, the RclA C43S crystals were incubated in a reservoir solution supplemented with 5 mM $CuCl_2$ for 15 h. After incubation of the crystals in reservoir solution supplemented with 30% (v/v) glycerol and 5 mM $CuCl_2$ for 30 s, crystals were flash-frozen in a nitrogen stream at –173°C.

2.5. Data collection and structural determination

All diffraction datasets were collected at the Pohang Accelerator Laboratory Beamline 5C (20) and were processed using the HKL-2000 package (21,22). The structure of the RclA wild type was determined using the molecular replacement method with MOLREP in the CCP4 package (22), using a model built by the Galaxy web server (23,24) as a search model. The initial model of the RclA wild type was used to solve structures of RclA wild type in complex with Cu^{2+} and RclA (C43S) in complex with Cu^{2+} by the molecular replacement method. All of the structures were built using COOT and refined using PHENIX refine software (25,26). The detailed statistics are shown in Table 1.

2.6. Enzyme kinetic assays

All assays were performed using UV-Vis spectrophotometer, GeneQuant 1300 (GE Healthcare) or Thermo Scientific Multiscan Go (Thermo Fisher Scientific). The RclA activity was assayed by adding 2 μM protein (as measured based on flavin content) in 10 mM MES buffer (pH 7.0) containing 100 mM NaCl, 0.2 mM NADH, and 0.2 mM putative substrate. Initial rates of NADH oxidation by RclA with various metal ions were monitored by the loss of absorbance at 340 nm due to NADH oxidation ($\Delta\varepsilon_{340}$ = 6.2 mM^{-1} cm^{-1}); loss of absorbance was monitored for 10 min and the oxidation profile was expressed in a time-dependent manner as the mean ± standard deviation (SD) of three independent experiments. Control assays lacking the substrate or enzyme were routinely included as references. NADH oxidation by RclA mutants C43S and C48S were recorded as previously described for the RclA wild type assay.

For the examination of enzyme dependency on Cu^{2+} concentration, NADH oxidation was measured at 340 nm with various concentrations of $CuCl_2$. Before the assay, the RclA wild-type protein was desalted with 10 mM MES buffer (pH 7.0) supplemented with 100 mM NaCl to remove any remaining 2-mercaptoethanol from the RclA size exclusion chromatography buffer. The activity assays were initiated by adding 2 μM desalted RclA wild-type protein to 10 mM MES buffer (pH 7.0) containing 100 mM NaCl, 0.2 mM NADH, and 0, 0.025, 0.05, 0.075, 0.1, 0.2, or 0.3 mM $CuCl_2$. Initial rates

were monitored by the loss of absorbance at 340 nm due to NADH oxidation ($\Delta\varepsilon_{340}$ = 6.2 mM^{-1} cm^{-1}) and expressed as the mean ± SD of four independent experiments.

2.7. NADH oxidation assay under low O_2 conditions

The dissolved oxygen (DO) was removed by nitrogen purging. The buffer with 10 mM MES (pH 7.0), 100 mM NaCl, 0.2 mM NADH, and with or without 0.1 mM $CuCl_2$ was contained in 1 mL cuvette and sealed with parafilm. The solution was purged with N_2 for 5 min. After nitrogen purging, 2 μM of RclA was added. Initial rates of NADH oxidation by RclA were monitored by the loss of absorbance at 340 nm due to NADH oxidation ($\Delta\varepsilon_{340}$ = 6.2 mM^{-1} cm^{-1}) was monitored using a GeneQuant 1300 UV-Vis spectrophotometer (GE Healthcare) and was expressed in time-dependent manner as the mean ± standard deviation (SD) of three independent experiments. A control assay in which the solution was not purged with N_2 was included for comparison.

2.8. Detection of DO in water

DO concentrations were measured using the Gravity Analog Dissolved Oxygen Sensor (SKU:SEN0237; DFRobot) with an Arduino Nano board and the Arduino IDE program (27). The programming code was obtained from the DFRobot website (https://wiki.dfrobot.com/Gravity_Analog_Dissolved_

Oxygen_Sensor_SKU_SEN0237). The reaction volume was 5 mL, containing 10 mM MES (pH 7.0) buffer with 100 mM NaCl, 0.2 mM NADH, and 1 μM RclA, with or without 0.2 mM $CuCl_2$. The solution was stirred gently with a 1 cm magnetic stir bar to distribute DO evenly throughout the entire solution. After pre-incubation for 5 min with stirring for equilibrium, the RclA protein was added and the DO concentration was recorded for 10 min. The specific oxidation rate was measured within the initial 1 min and is expressed as the mean ± SD of three independent experiments.

2.9. Measurement of $O_2^{\bullet -}$ formation by cytochrome C assay

Superoxide anion ($O_2^{\bullet -}$) formation was determined by monitoring the reduction of cytochrome C, which was isolated from the equine heart (Sigma Aldrich). The reaction was performed with 200 μL buffer containing 10 mM MES buffer (pH 7.0), 100 mM NaCl, 200 μM NADH, 100 μM $CuCl_2$, 2 μM RclA, and 50 μM cytochrome C. The increase in the absorbance at 550 nm due to cytochrome C reduction was recorded at 37°C for 10 min using a UV-Vis spectrophotometer (Thermo Scientific Multiscan Go). The amount of $O_2^{\bullet -}$ released was calculated using an extinction coefficient of 21 mM^{-1} cm^{-1} and expressed as the mean ± SD of three independent experiments.

III. Results

3.1. Overexpression and Purification of RclA wild type

RclA is commonly found in *Salmonella* and *E. coli*. Since HOCl is produced in macrophage phagosomes as a major bactericidal agent, the function of RclA in resistance to HOCl suggests that RclA plays a role in the survival of the bacteria. Previous unpublished data from the Molecular Food Microbiology Lab of Seoul National University showed that RclA is involved in the pathogenesis of *Salmonella* by promoting survival in macrophage vacuoles containing sublethal doses of HOCl.

Sequence comparison suggested that RclA belongs to the group I FDRs due to the presence of two important motifs; CXXXXC for the redox-active disulfide as a non-flavin redox center, and the essential HXXXXE which interacts with and promotes the disulfide formation of the CXXXXC motif with its histidine residue (18) (Fig. 1 and Fig. 2).

To gain mechanistic insights on RclA from its 3D structures, the full-length RclA proteins (441 amino acids) of *E. coli* was overexpressed and purified through affinity chromatography, anion exchange chromatography, and size exclusion chromatography. (Fig. 3) Each step was monitored by SDS-PAGE.

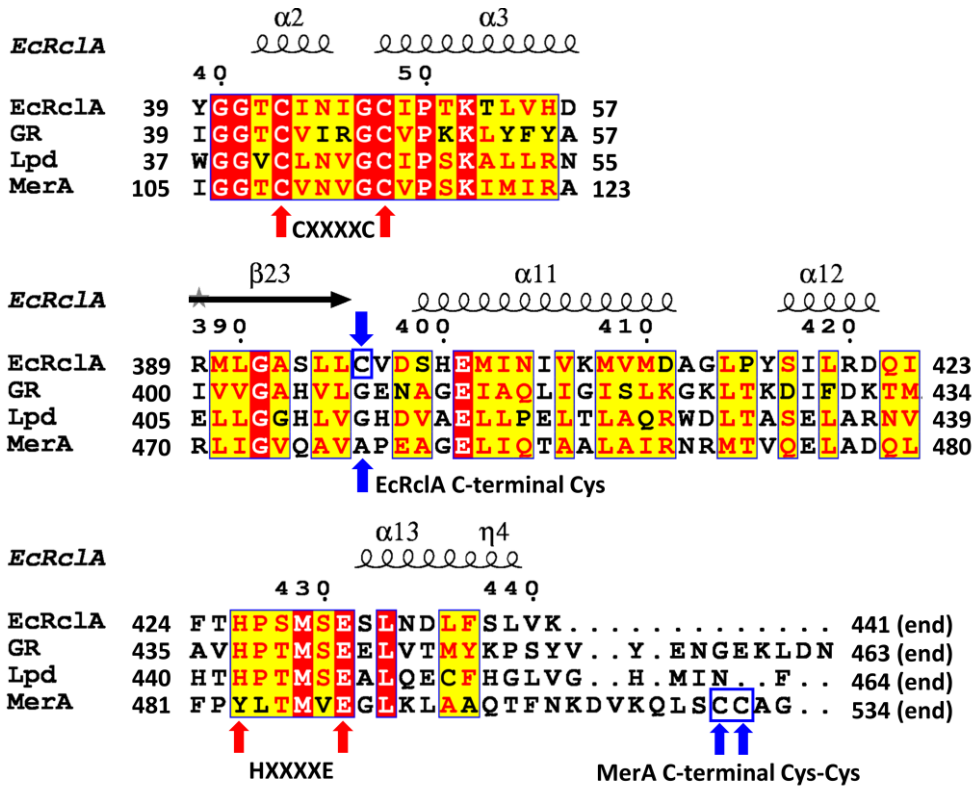

Figure 1. Sequence analyses and crystal structure of EcRclA

Sequence alignment of FDR proteins with the secondary structure elements. For clarity, the regions containing the signature motifs are displayed. The full sequence alignment is presented in Figure 2. The cysteine residues in the CXXXXC motifs and histidine and glutamate residues in the HXXXXE motif are indicated by red arrows. The C-terminal Cys in EcRclA and the C-terminal Cys-Cys motif in MerA are indicated by blue arrows and blue square.

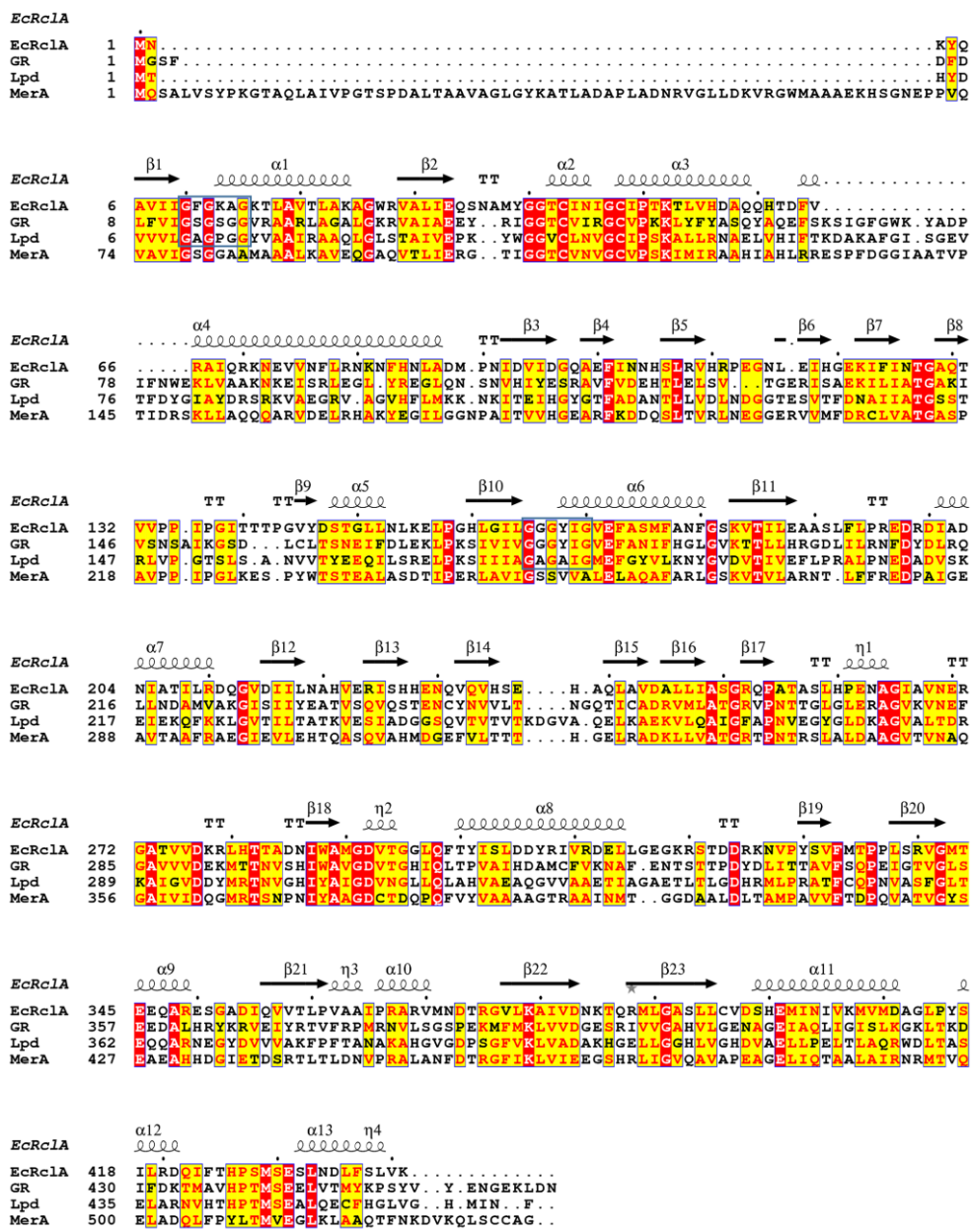

Figure 2. Full sequence alignment of EcRclA and representative FDR proteins with the secondary structure elements.

GR; glutathione-disulfide reductase from *Bartonella henselae*, (GenBank: WP_011180567), Lpd; dihydrolipoyl dehydrogenase from mycobacterium multispecies (GenBank: WP_003402301.1), MerA; mercuric reductase from

Pseudomonas aeruginosa (GenBank: WP_023980594.1). The sequence alignment was performed using the T-Coffee server (28) and the ESPript server (29).

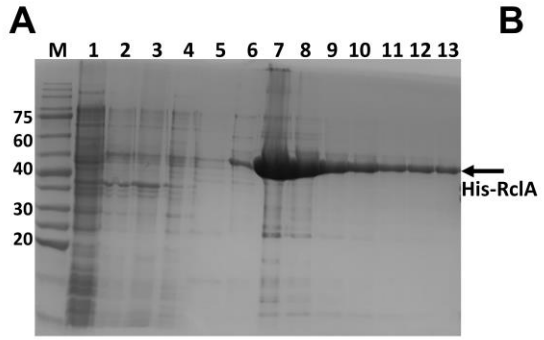

Lane 1: Before induction
Lane 2: Supernatant fraction
Lane 3: Precipitant fraction
Lane 4: Unbound fraction
Lane 5: Washed fraction
Lane 6-13: Eluted fraction

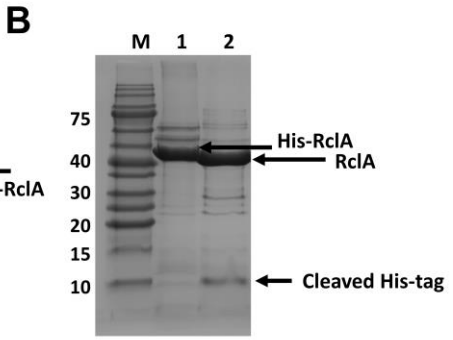

Lane 1: Before TEV protease cleavage
Lane 2: After TEV protease cleavage

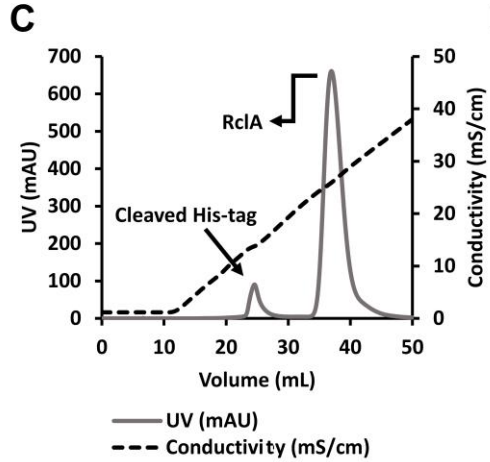

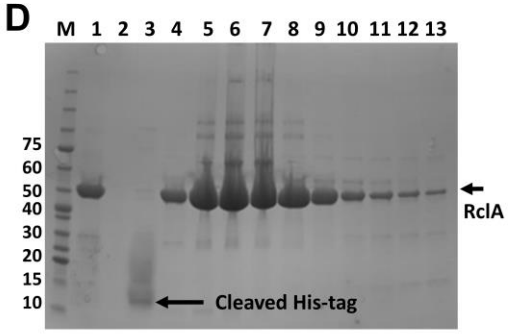

Lane 1: Before anion exchange chromatography
Lane 2: Q-column unbound fraction
Lane 3: Eluted fraction of cleaved His-tag
Lane 4-13: Eluted fraction of RclA

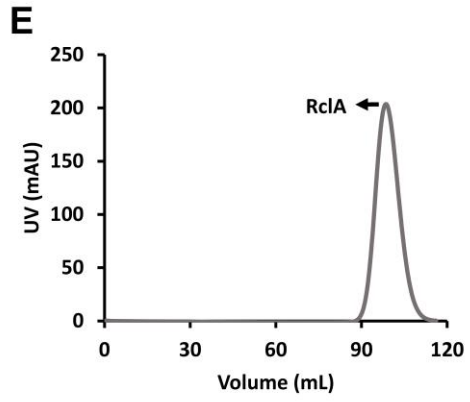

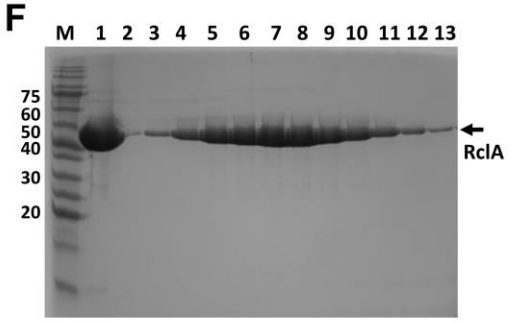

Lane 1: Before size exclusion chromatography
Lane 2-13: Eluted fraction of RclA

Figure 3. Purification profile of RclA wild type.

A. The SDS-PAGE analysis of Ni-NTA affinity chromatography

B. The SDS-PAGE analysis of His-tag cleavage using TEV protease.

C. UV and conductivity diagram of the Q-column elution during the anion exchange chromatography.

D. The SDS-PAGE analysis of anion exchange chromatography

E. UV diagram of the superdex column elution during the size exclusion chromatography.

F. The SDS-PAGE analysis of size exclusion chromatography.

3.2. Crystallization, structural determination and overall structure of EcRclA wild type

The purified RclA wild type was concentrated up to 13 mg/mL for the crystallization. The crystals of RclA wild type were obtained in the precipitant solution containing 0.2 M ammonium sulfate, 0.1 M Bis-Tris HCl (pH 6.5), 25% (w/v) PEG 3350. Optimizing the precipitant solution to 0.2 M ammonium sulfate, 0.1 M Bis-Tris HCl (pH 5.8), 13% (w/v) PEG 3350, and 2 mM TCEP improved the quality of RclA crystals (Fig. 4).

The crystal structure of RclA from *E. coli* (EcRclA) was successfully determined at 2.9 Å resolution (Fig. 4 and Table 1). The crystal of RclA belongs to the space group $P2_1$, with unit cell dimensions of a=72.4 Å, b=189.4 Å, and c=95.4 Å. The asymmetric unit contained four protomers consisting of two homodimers (Fig. 5). Each protomer contained a tightly bound FAD molecule in its active site (Fig. 6).

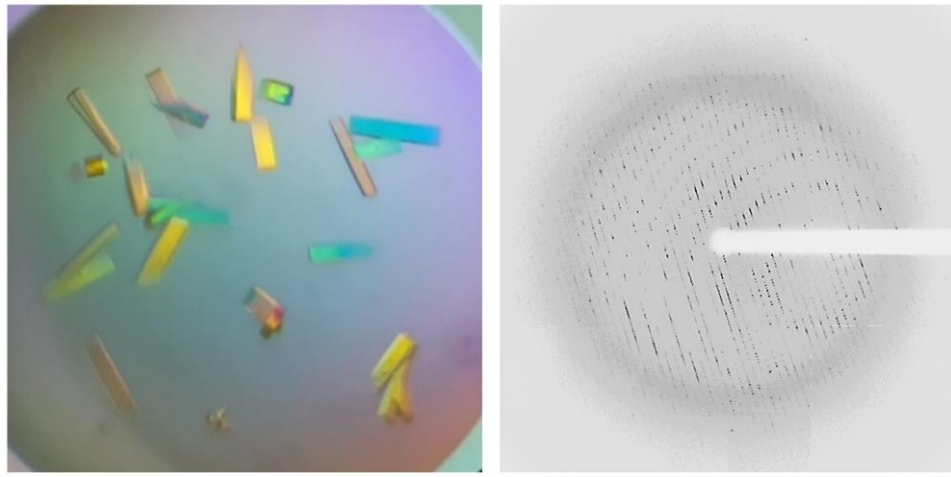

Figure 4. Crystals (left) and X-ray diffraction image (right) of RclA wild type.

Table 1. Data collection and refinement statistics

	RclA wild type	RclA wild type (Cu^{2+})	RclA C43S (Cu^{2+})
Data collection			
Beam line	PAL 5C	PAL 5C	PAL 5C
Wavelength (Å)	0.97960	1.00003	1.00003
Space group	$P2_1$	$P2_1$	$P2_1$
Cell dimensions			
a, b, c (Å)	72.4, 189.4, 95.4	72.6, 188.4, 95.0	72.8, 191.5, 95.2
α, β, γ (°)	90, 107.3, 90	90, 107.6, 90	90, 107.4, 90
Resolution (Å)	50.0–2.90 (2.95–2.90)	50.0–2.80 (2.85–2.80)	50.0–3.00 (3.05–3.00)
R_{pim}	0.044 (0.144)	0.042 (0.198)	0.045 (0.163)
R_{merge}	0.117 (0.281)	0.065 (0.374)	0.087 (0.235)
I/σ	12.3 (4.21)	17.4 (4.4)	10.7 (2.7)
Completeness (%)	98.5 (95.2)	99.4 (97.6)	92.8 (82.1)
Redundancy	5.0 (3.2)	3.6 (3.3)	3.7 (2.3)
Refinement			
Resolution (Å)	40.37–2.9	47.24–2.8	46.61–3.0
No. reflections	54,069	81985	45,241
R_{work}/R_{free}	0.2346/0.2806	0.2226/0.2707	0.2081/0.2565
No. of total atoms	13,746	13,709	13,845
Wilson B-factor (Å)	43.62	33.08	51.40
R.M.S deviations			
Bond lengths (Å)	0.002	0.003	0.002
Bond angles (°)	0.511	0.520	0.516
Ramachandran plot			
Favored (%)	94.5	95.41	95.67
Allowed (%)	5.5	4.59	4.33
Outliers (%)	0.0	0.0	0.0
PDB ID	6KGY	6KYY	6KOD

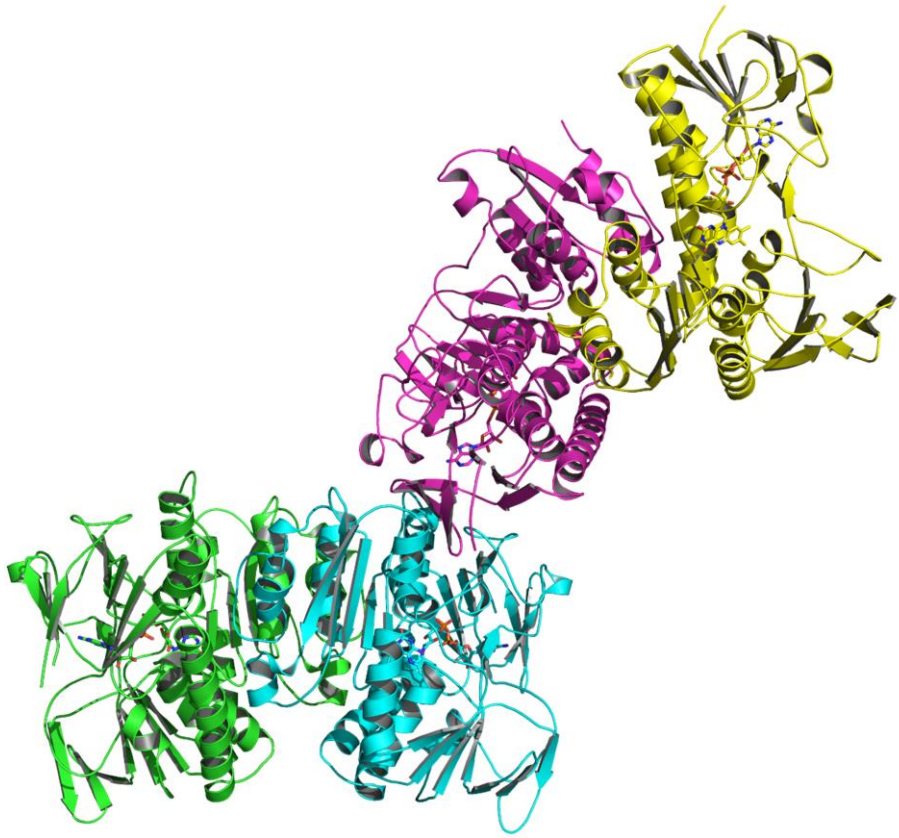

Figure 5. The structure of the asymmetric unit of RclA in the ribbon representations.

The asymmetric unit consists of four protomers, which are colored differently (green, cyan, magenta, and yellow). The bound FAD molecules are shown in the stick representations.

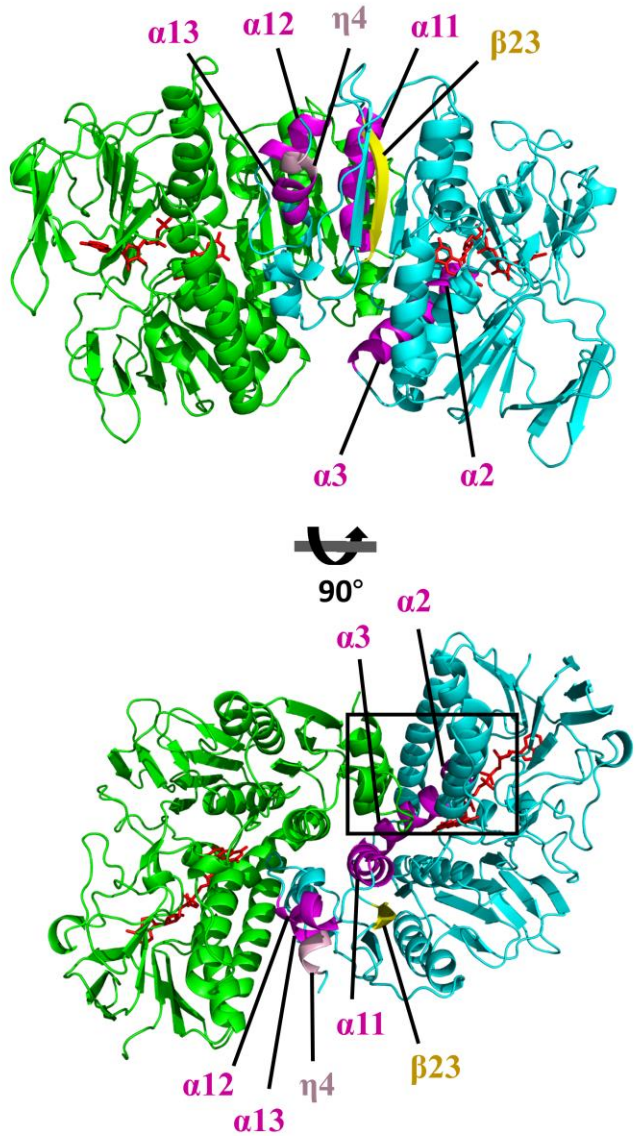

Figure 6. The overall structure of EcRclA.

The subunits are depicted by the ribbon representations in cyan (subunit A) or green (subunit B). Secondary structure elements shown in Figure 2A are indicated with a different color in subunit A. α2, α3, α12, α13 are in magenta. β23 is in yellow, and η4 is in pink. The bound FAD molecules are shown in the red stick representations. The boxed region is enlarged in Figure 7.

3.3. Structural comparison to group I FDRs

The overall arrangement of the CXXXXC and HXXXXE motifs in the active sites is similar to that of group I FDR family proteins (Fig. 7 and Fig. 8). The two cysteines in the CXXXXC motif are in the reduced form and the distance between the sulfur atoms of the two cysteine residues is ~4.4 Å in the crystal structure. The two cysteine residues are near the isoalloxazine ring of FAD, and Cys48 is closer to FAD than to Cys43 (the distance between the Sγ of Cys48 and the C4a atom of flavin is 3.5 Å). The HXXXXE motif from the other subunit in the dimer is involved in the interaction with the CXXXXC motif and the bound FAD (Fig. 8). His426 and Glu431 are paired with a distance of 2.5 Å, and His426 makes a polar interaction with Cys43 (Fig. 7). Remarkably, two lysine residues (Lys13 and Lys16), which are unique to RclA proteins, were found near Cys43 at the active site. Because group I FDR proteins reduce substrates via the disulfide formation of the CXXXXC motif together with the HXXXXE motif, our findings suggest that RclA shares the enzymatic mechanism of group I FDR proteins.

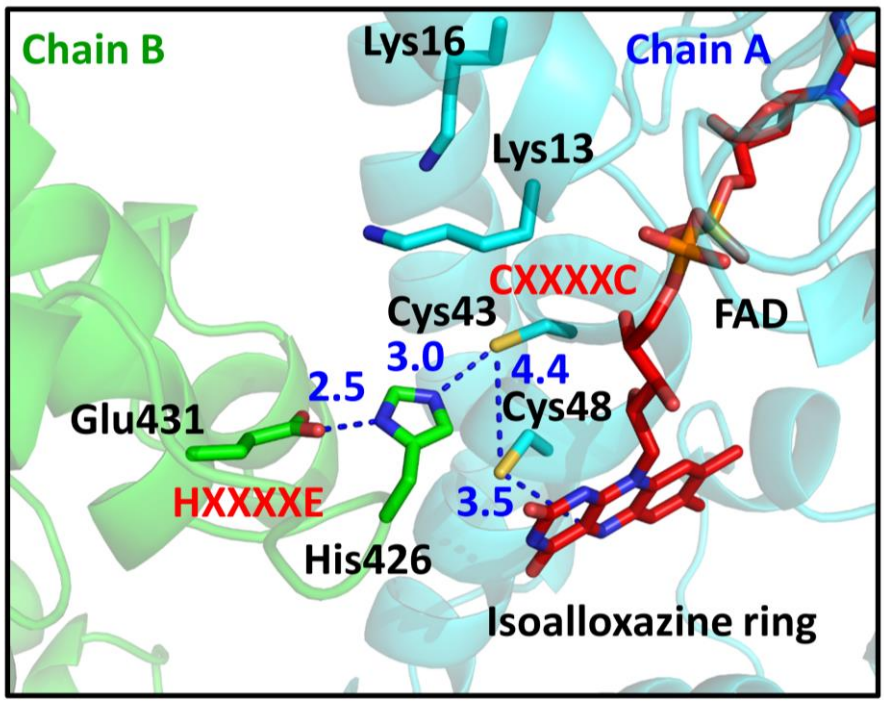

Figure 7. The structure of the active site of EcRclA.

The active site of RclA. The box is enlarged from Figure 6. Each subunit is depicted by the ribbon representation in green or cyan. The bound FAD molecules are shown in the red stick representations. Each residue and FAD are labeled and indicated in the stick representations with the ribbon diagram in the background. The key interactions between the two cysteines of CXXXXC, His426, and Glu431 of HXXXXE, and Cys48 and the C4a atom of FAD are shown in blue dotted lines. Distances are in Å (Blue).

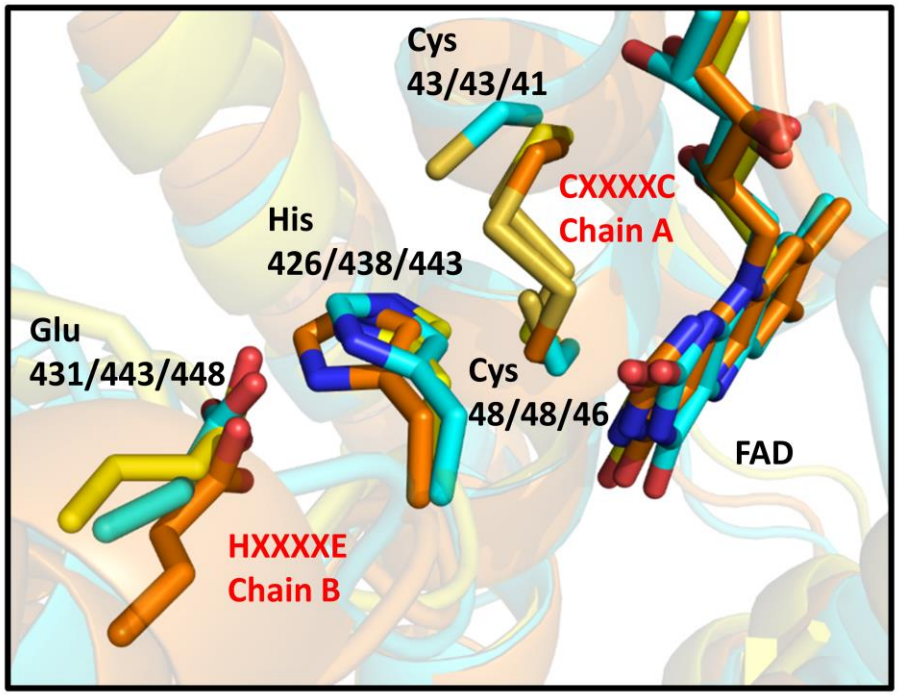

Figure 8. Structural superposition of EcRclA (cyan) with the group I FDR proteins.

Glutathione reductase (orange, PDB ID: 3O0H) and lipoamide dehydrogenase (yellow, PDB ID: 4M52) were ranked as top entries from the DALI server structural analyses, following MerA. The conserved CXXXXC and HXXXXE motifs are labeled in red. Each residue depicted in stick representation is labeled with residue numbers of three proteins (first RclA, second 3O0H, third 4M52).

3.4. Structural comparison to the group II FDR MerA

I searched for the closest protein to RclA in terms of structure using the DALI server (30). Mercuric reductase (MerA) (PDB code: 4K7Z), a group II FDR, was ranked as the top entry (Z-score: 43.6). Like EcRclA reduces Cu^{2+} to Cu^{+}, MerA converts Hg^{2+} to Hg^{0} (18). MerA contains the CXXXXC motif, similar to group I FDR proteins, and tyrosine replaces the histidine residue in the HXXXXE motif (Fig. 1). The structural superposition of EcRclA onto MerA revealed a strong structural similarity between the matched regions (sequence identity: 30%, RMSD: 1.522 between 320 Cα atoms, residues 5–433 of EcRclA), except for the Cys-Cys motif for metal ion binding (Fig. 9 and Fig. 10). The C-terminal end loop containing the Cys-Cys motif was folded into the active site near the CXXXXC motif and the tyrosine residue in the MerA structure (Figs. 1 and 10). The Cys-Cys motif and the tyrosine residue interact with a mercuric ion at the active site (31).

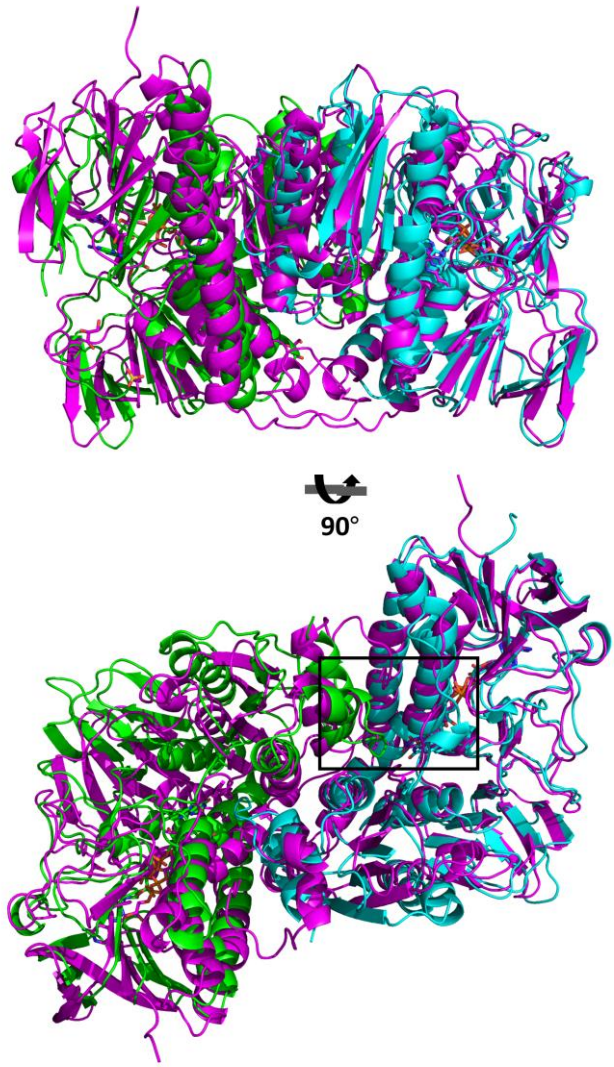

Figure 9. Overall superposition between RclA (green and cyan) and MerA (magenta, PDB ID: 4K7Z), which are in dimeric forms.

The boxed region is enlarged in Figure 10. Sequence identity: 30%, RMSD: 1.522 between 320 Cα atoms, residues 5–433 of EcRclA

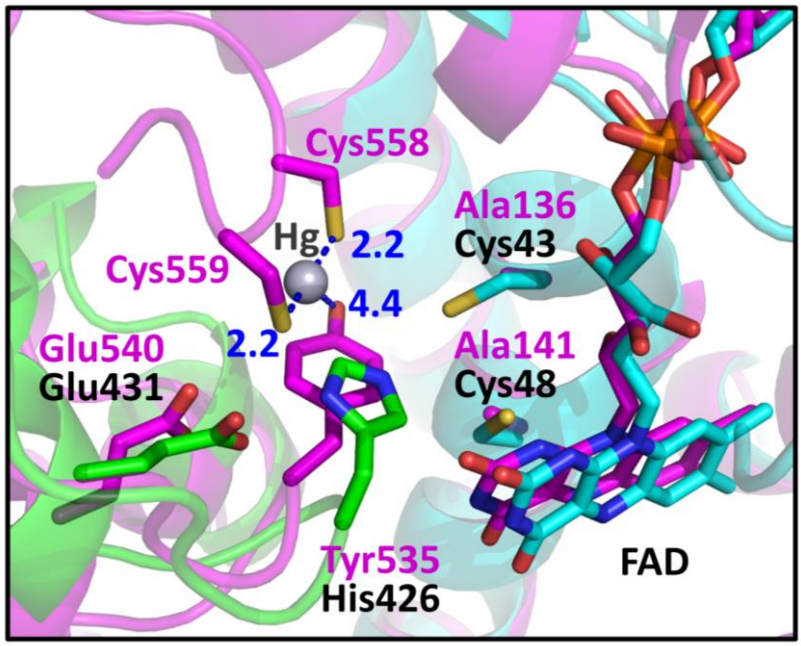

Figure 10. Active site comparison with MerA.

The box is enlarged from Figure 9. RclA (green, cyan) is aligned with MerA (magenta, PDB ID:4K7Z) (32). Each residue aligned in the active site is labeled in a different color (black for RclA and magenta for MerA). His426 in RclA is substituted with Tyr535 in MerA. Mercury was bound to the two C-terminal cysteines of MerA, Cys558, and Cys559. The interactions between the mercury, cysteine, and histidine residues are depicted in dashed lines. The two cysteine residues in the CXXXXC motif of MerA were substituted with alanine to determine the Hg^{2+}-bound structure (32). Distances are in Å (Blue).

3.5. Cu^{2+} and Hg^{2+} accelerate the oxidation of NADH in RclA

To elucidate the mechanism of RclA, further biochemical analyses were performed. Initially, the basal level of the NADH oxidase activity of RclA was observed (Fig. 11A and B), which is found in many FDR enzymes (33-35). Previous studies of other FDRs suggested that the basal activity of RclA resulted from oxidation by the molecular oxygen in the buffer (33,35-37). Next, RclA was tested whether it exhibits the MerA-like activity in which NADH oxidase activity is increased by adding metal ion (38,39). The NADH oxidase activity of RclA was measured in the presence of diverse metal ions, such as Hg^{2+}, Cu^{2+}, Fe^{3+}, Mn^{2+}, Mg^{2+}, and Zn^{2+} (Fig. 11A). Notably, Hg^{2+} and Cu^{2+} increased oxidation of NADH by approximately three-fold compared to the basal activity without the metal ions, and Ag^{+} resulted in an approximately two-fold increase. However, Fe^{2+}, Mg^{2+}, Zn^{2+}, and Mn^{2+} did not affect the NADH oxidase activity. Cu^{2+} accelerated the NADH oxidation rate in a dose-dependent manner until reaching 0.3 mM $CuCl_2$ (Fig. 11B and C).

To identify other substrates, the NADH oxidation activity was tested with oxidized glutathione (GSSG), lipoic acid, cystine, and HOCl, which could be putative substrates of RclA. No increase was observed in the NADH oxidation rate by RclA with these substances (Fig. 11D). Cu^{2+} was used in the following analyses because Hg^{2+} and Ag^{+} are not relevant in host immune responses and Cu^{2+} is employed in phagosomes of host innate immune systems.

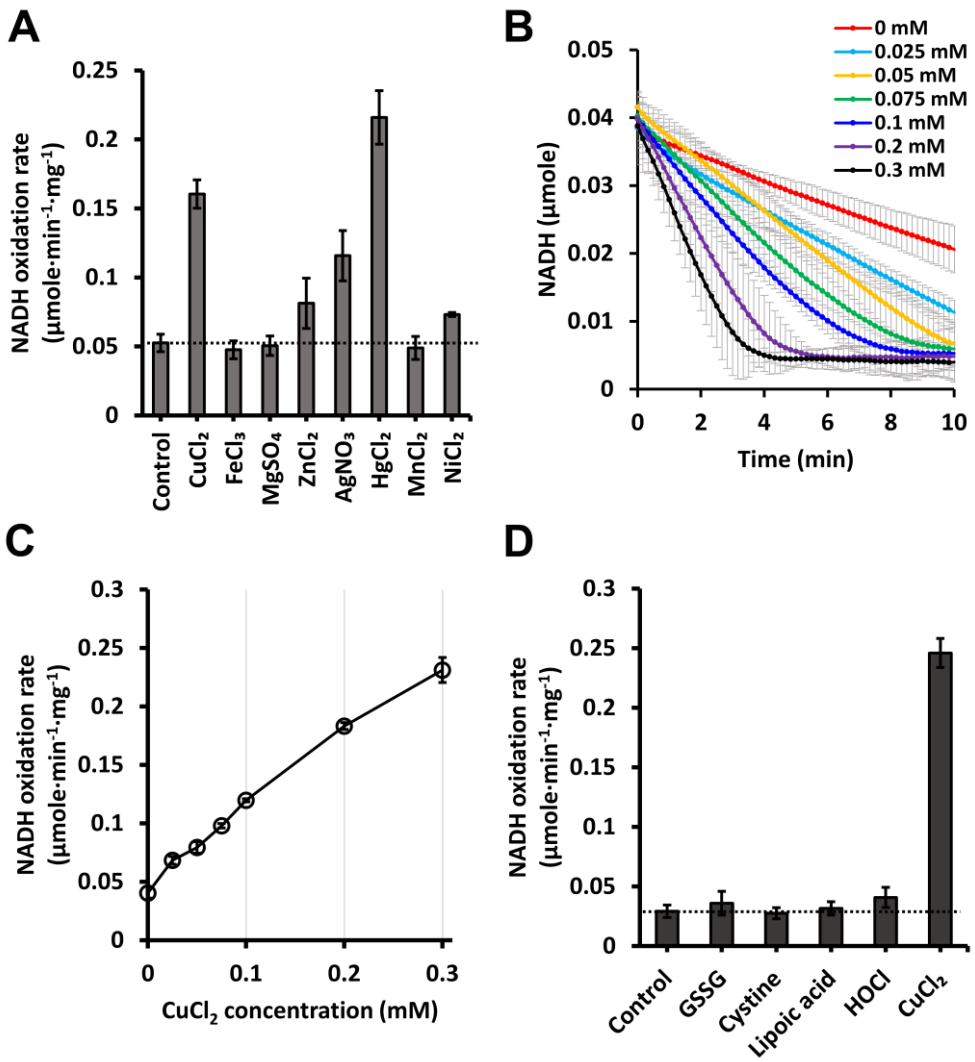

Figure 11. The NADH oxidation rates by EcRclA in the presence of various substrates

A. NADH oxidation rates depending on various transition metal ions. NADH oxidation rates by RclA were measured over time spectrophotometrically (n = 3, mean ± SD). The reaction was initiated by injecting 200 μM NADH into a buffer containing 2 μM RclA with or without 100 μM of metal ions. A control experiment was performed without metal ion. The horizontal line indicates the reference NADH oxidation rate of control.

B. NADH oxidation profile with different concentrations of Cu^{2+}. The reaction was assayed with 200 μM NADH and marked concentrations of $CuCl_2$ (from 0 mM to 0.3 mM). The amounts of the NADH oxidation were measured spectrophotometrically (n = 3, mean ± SD).

C. Initial NADH oxidation rates calculated from the NADH oxidation profile in Figure 4B. The reaction was assayed with 200 μM NADH and marked concentrations of Cu^{2+}. The NADH oxidation rates were measured over time spectrophotometrically (n = 3, mean ± SD).

D. NADH oxidation rate with various substances. The reaction was initiated by injecting 200 μM NADH into a buffer containing 2 μM RclA and 200 μM of various materials. A control experiment was performed without material. NADH oxidation rates were measured over time spectrophotometrically (n = 3, mean ± SD)

3.6. O_2 is required for NADH oxidation in the presence of Cu^{2+}

Although Derke *et al*. reported the reduction of Cu^{2+} with the reducing power of NADH (17), the redox stoichiometry was not completely accounted for. Only 25% of the reducing power from NADH was used in the Cu^{2+} reduction to produce Cu^{+} (Fig. 4B in (17)). Given that molecular oxygen dissolved in the reaction buffer is the oxidant candidate, molecular oxygen was investigated as the second oxidant in the RclA-mediated reaction.

Because a significant amount of O_2 is dissolved in ambient conditions, the NADH oxidase activity of RclA was investigated under oxygen-depleted conditions by thoroughly purging the buffer with nitrogen gas (Fig. 12A). The NADH oxidation rate of EcRclA was compared in the presence and absence of Cu^{2+}. The depletion of dissolved oxygen almost completely shut down the NADH oxidation by RclA regardless of the presence of Cu^{2+}. Stoichiometric analyses of this reaction accounted for 50% of the NADH oxidation in the presence of Cu^{2+}. Thus, our findings suggest that the presence of Cu^{2+} and molecular oxygen are interlinked in the oxidation of NADH by RclA, and O_2 is required for Cu^{2+}-mediated NADH oxidation by RclA.

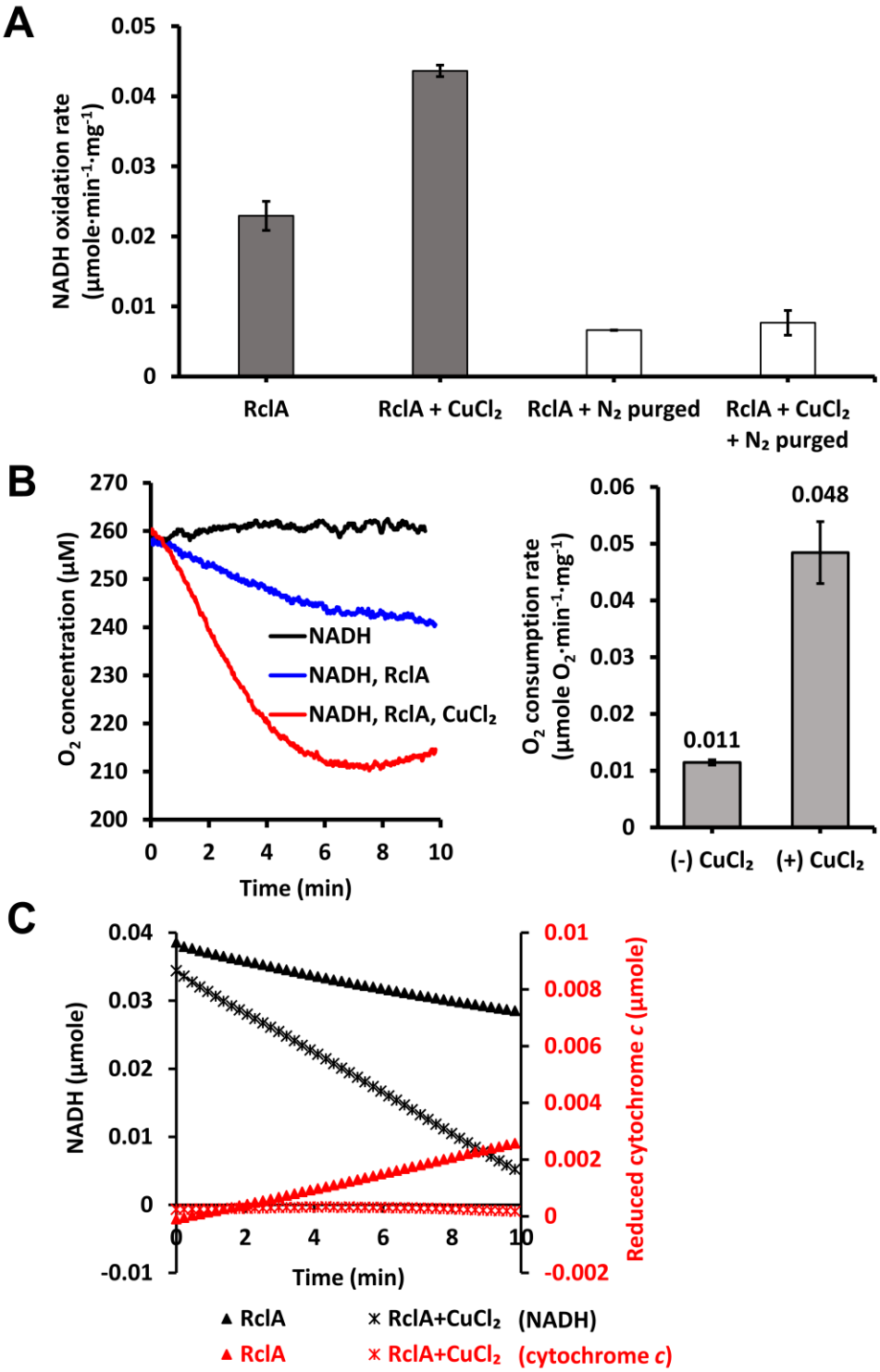
A
NADH oxidation rate (μmole·min-1·mg-1)
0.05
0.04
0.03
0.02
0.01
0
RclA
RclA + CuCl2
RclA + N2 purged
RclA + CuCl2 + N2 purged
B
O2 concentration (μM)
270
260
250
240
230
220
210
200
0
2
4
6
8
10
Time (min)
NADH
NADH, RclA
NADH, RclA, CuCl2
O2 consumption rate (μmole O2·min-1·mg-1)
0.06
0.05
0.04
0.03
0.02
0.01
0
0.048
0.011
(-) CuCl2
(+) CuCl2
C
NADH (μmole)
0.04
0.03
0.02
0.01
0
-0.01
Reduced cytochrome c (μmole)
0.01
0.008
0.006
0.004
0.002
0
-0.002
0
2
4
6
8
10
Time (min)
RclA
RclA+CuCl2 (NADH)
RclA
RclA+CuCl2 (cytochrome c)

Figure 12. O_2 depletion and consumption during NADH oxidation by EcRclA

A. NADH oxidation by RclA in O_2-depleted conditions. The oxidation rates were measured with 200 μM NADH, 2 μM EcRclA wild type, and with or without 100 μM $CuCl_2$ over time spectrophotometrically (n = 3, mean ± SD). O_2 depletion was performed via N_2 purging.

B. O_2 consumption during the NADH oxidation reaction by RclA. Left, O_2 consumption profile during the NADH oxidation reaction. The reaction was initiated by the addition of 200 μM NADH into the pre-incubated reaction solution containing 200 μM Cu^{2+} and 2 μM RclA. The O_2 concentrations in the buffer were measured over time with the Arduino dissolved oxygen sensor. Data are the averages of three independent experiments. Right, O_2 consumption rates during the NADH oxidation reaction with RclA and Cu^{2+}. The O_2 consumption rates were measured over time (n = 3, mean ± SD).

C. Superoxide anion production during NADH oxidation by EcRclA wild type. Superoxide anion production was measured based on the amount of reduced cytochrome *c* at 550 nm (line), and NADH oxidation was measured at 340 nm (dotted line) over time spectrophotometrically. The reaction was performed in the presence or absence of 100 μM Cu^{2+} in buffer containing 200 μM NADH and 2 μM EcRclA wild type. Data are the averages of three independent experiments.

3.7. Cu^{2+} promotes O_2 consumption without producing superoxide anion

To determine whether O_2 was used as the oxidant during the RclA reaction, the amount of oxygen dissolved in the reaction buffer was measured with an oxygen probe during oxidation of NADH by RclA (Fig. 12B). The specific O_2 consumption rate in the presence of 200 μM Cu^{2+} was about four times faster than that in the absence of Cu^{2+} (Fig. 12B), as observed in the NADH oxidation rates in the presence and absence of Cu^{2+} (Fig. 11C). These results indicate that Cu^{2+} catalyzes the reduction of oxygen during the oxidation of NADH. About 50 μM oxygen was consumed by the time 200 μM NADH was used completely in the reaction (Fig. 12B and 11B), indicating that four NADH molecules were required for one oxygen molecule in this reaction of RclA.

Many FDR enzymes produce superoxide anion as the basal or side activity by a reaction between the bound $FADH_2$ and molecular oxygen (36). Therefore, the amount of superoxide anion produced in the RclA-mediated reaction without Cu^{2+} was measured using cytochrome C, which is rapidly reduced by superoxide anion with an increase in light absorbance at 550 nm. Like other FDR enzymes, EcRclA without Cu^{2+} produced superoxide anion (Fig. 12C). Similar experiments were performed in the presence of Cu^{2+}. Production of superoxide anion was not observed in the reaction although more oxygen was consumed that in the absence of Cu^{2+} (Fig. 12C). These

findings indicate that Cu^{2+} promotes the reaction between oxygen and $FADH_2$ at the active site of RclA while suppressing the production of superoxide anion.

3.8. Overexpression and purification of RclA C43S and C48S

To investigate the roles of the two conserved cysteine residues (Cys43 and Cys48) in the CXXXXC motif and the additional cysteine residue (Cys396) at the C-terminus, mutant EcRclA proteins C43S, C48S, and C396S were produced. RclA C43S and C48S were overexpressed and purified through affinity chromatography, anion exchange chromatography, and size exclusion chromatography (Figs. 13 and 14). Each step was monitored by SDS-PAGE.

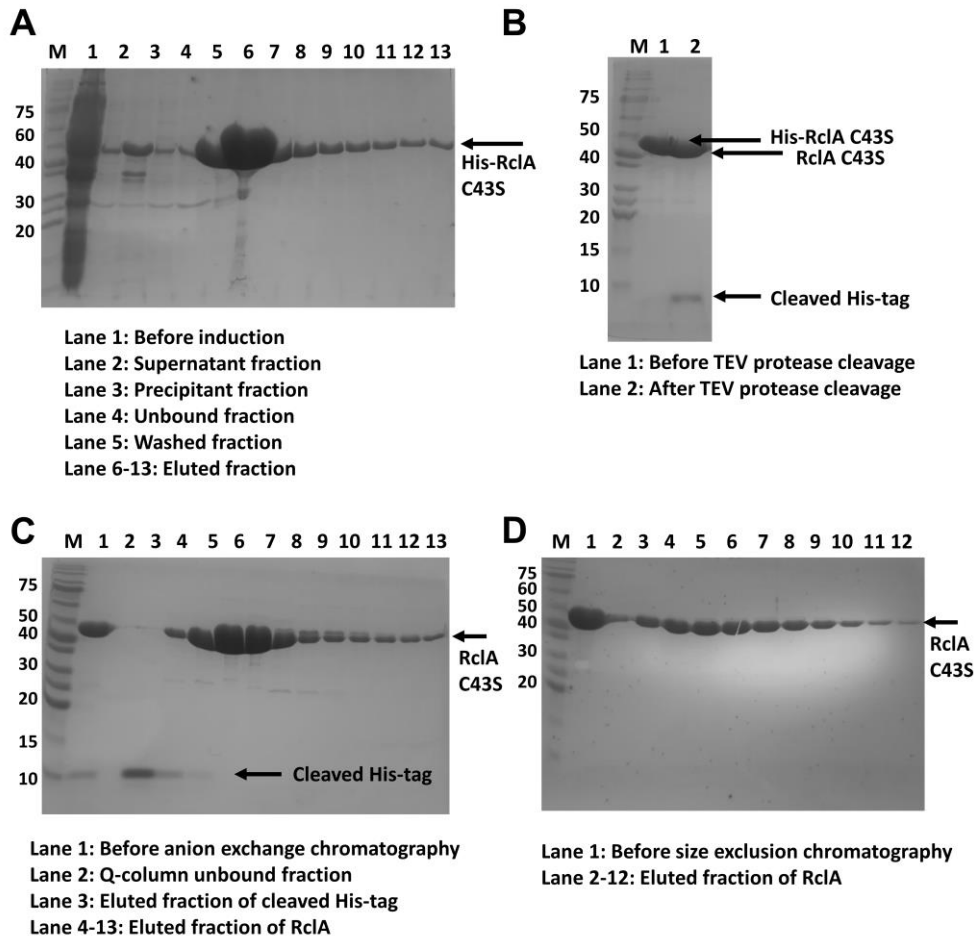

Figure 13. SDS-PAGE purification profile of RclA C43S.

A. The SDS-PAGE analysis of Ni-NTA affinity chromatography of RclA C43S. B. The SDS-PAGE analysis of His-tag cleavage using TEV protease of RclA C43S. C. The SDS-PAGE analysis of anion exchange chromatography of RclA C43S. D. The SDS-PAGE analysis of size exclusion chromatography of RclA C43S.

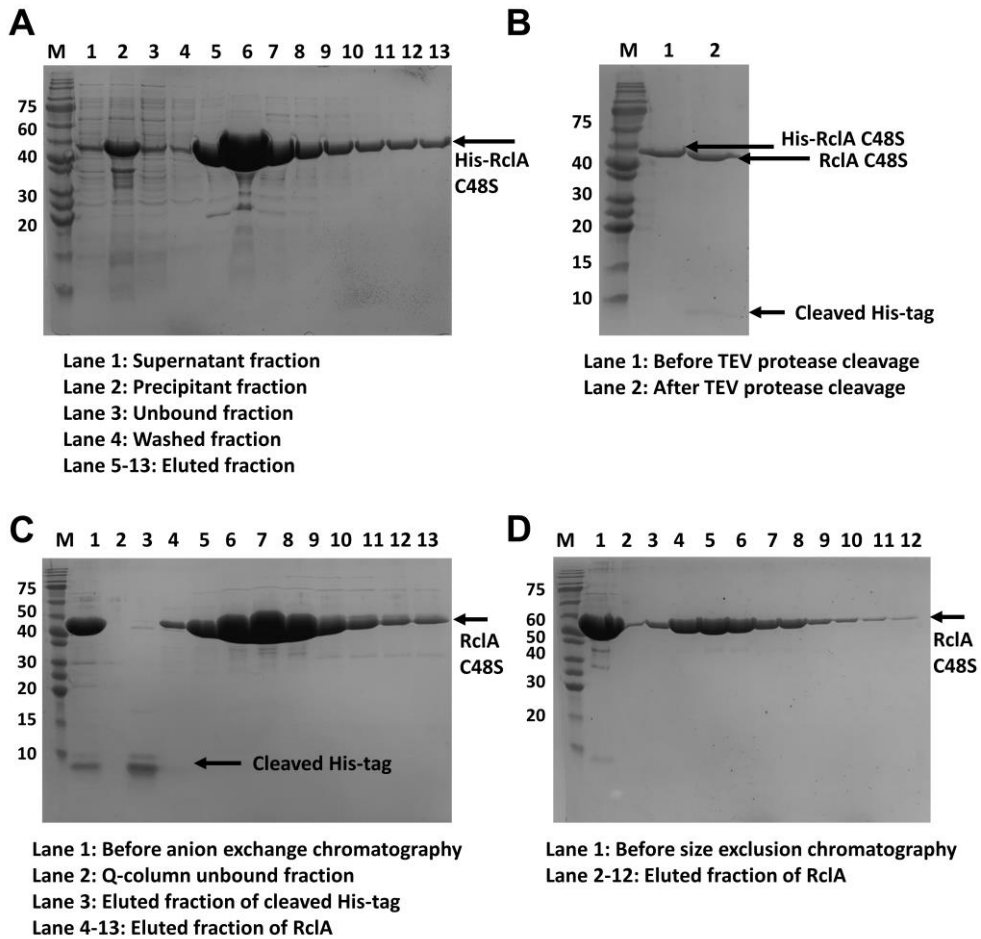

Figure 14. SDS-PAGE purification profile of RclA C48S.

A. The SDS-PAGE analysis of Ni-NTA affinity chromatography of RclA C48S. B. The SDS-PAGE analysis of His-tag cleavage using TEV protease of RclA C48S. C. The SDS-PAGE analysis of anion exchange chromatography of RclA C48S. D. The SDS-PAGE analysis of size exclusion chromatography of RclA C48S.

3.9. Roles of the two cysteine residues in the CXXXXC motif

To investigate the roles of the two conserved cysteine residues (Cys43 and Cys48) in the CXXXXC motif and the additional cysteine residue (Cys396) at the C-terminus, EcRclA C43S, C48S, and C396S were produced, and then tested their activities in the presence or absence of Cu^{2+}. The mutation at Cys396 did not affect the tested RclA properties (data not shown), which is consistent with the structural analyses. The cysteine residue was buried and surrounded by two methionine residues in the hydrophobic region in the crystal structure (Fig. 15). Because the cysteine residue is far from the active site, it is unlikely that Cys396 is involved in the catalysis.

However, analyses of the point mutation at Cys43 or Cys48 in the CXXXXC motif yielded interesting results (Fig. 16A). When Cys48 was changed to a serine, the NADH oxidase activity was highly increased regardless of the presence of Cu^{2+}, compared to those of wild-type enzyme (Fig. 16A and B). These observations indicate that the Cu^{2+}-dependent NADH oxidase activity of RclA is controlled by Cys48. In terms of production of superoxide anion, C48S showed the increased basal superoxide production rate in the absence of Cu^{2+}, indicating that Cys48 may contribute to the suppression of the basal superoxide production by RclA (Fig. 17).

The RclA C43S mutant showed a dramatic increase in NADH oxidase activity in the presence of Cu^{2+} compared to the wild type (Fig. 16A). However, the mutation at Cys43 increased the NADH oxidase activity in the

presence of other metal ions as well. Ag^{+} accelerated the oxidation rate of NADH as much as Cu^{2+}, and Zn^{2+} and Hg^{2+} also further increased the NADH oxidase activity compared to that of wild type enzyme (Fig. 16C). Thus our findings suggest that Cys43 is involved in the metal specificity and further in the binding of Cu^{2+} at the active site.

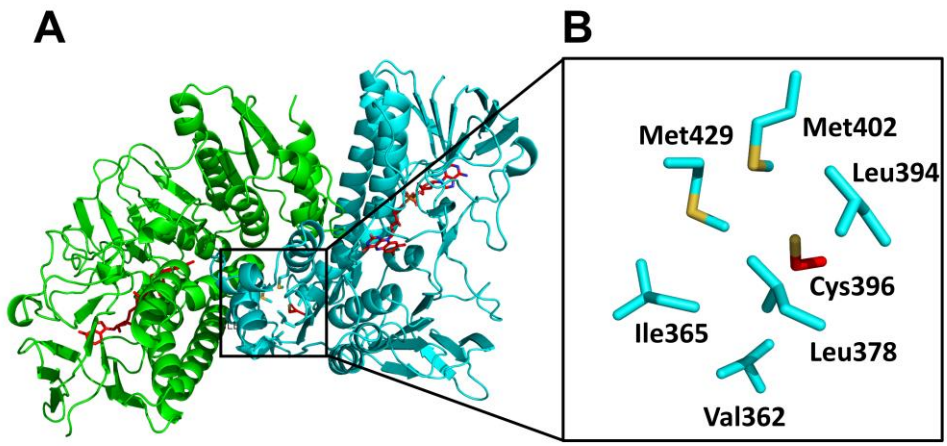

Figure 15. The location and the surrounding environment of Cys396 of EcRclA.

A. The overall structure of EcRclA in the near-top view. Each subunit is in a different color (cyan or green). The bound FADs are in the stick representations in red, which indicates the active sites. Cys396 and residues near Cys396 are shown in stick representation in the boxed region.

B. Cys396 and its surrounding residues, which are largely hydrophobic. The box is enlarged from the boxed region of A. The residues are represented in the stick model. The Cys396 residue is in red.

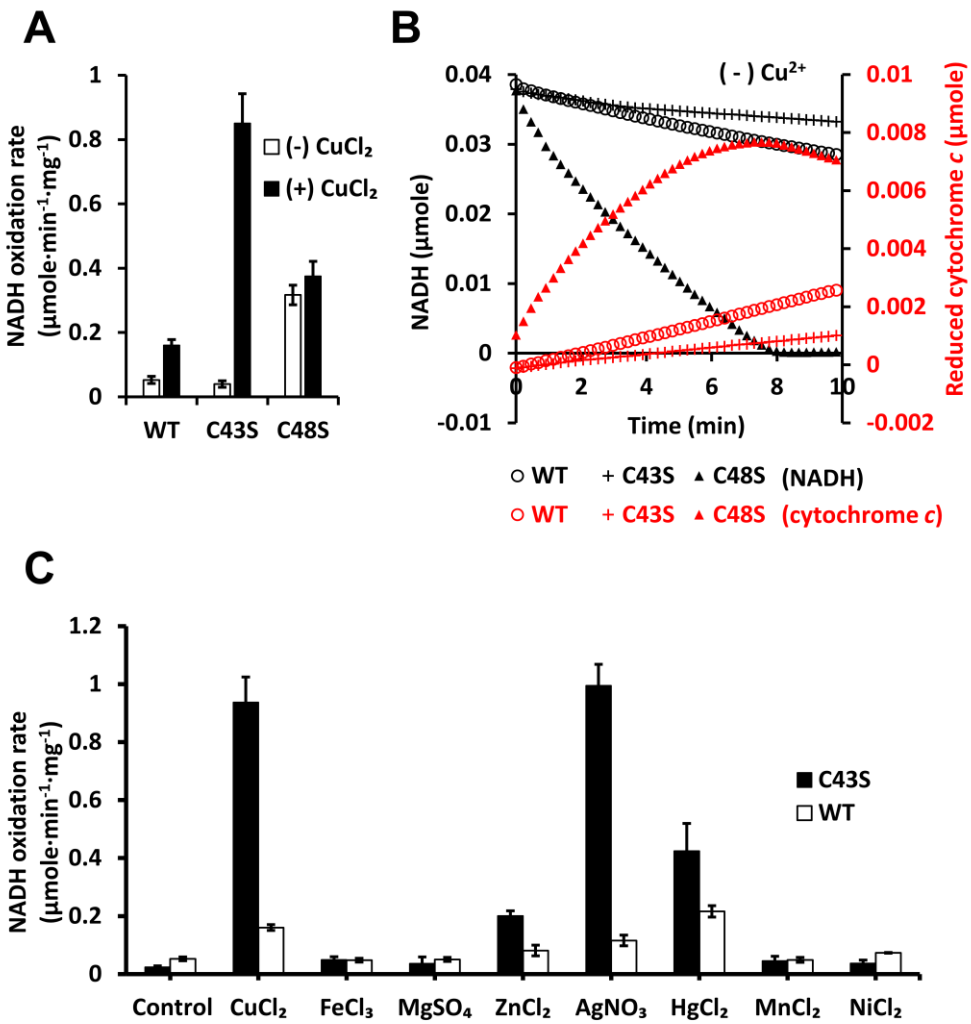

Figure 16. The activity of EcRclA mutants C43S and C48S compared to wild type

A. The initial NADH oxidation rate of RclA wild type (WT) and mutants. The reaction was performed with 200 μM NADH and 2 μM EcRclA, with or without 100 μM Cu^{2+}. Data are expressed as the mean ± SD of three independent experiments (μmole NADH ·min^{-1}·mg^{-1} RclA).

B. Superoxide anion production during NADH oxidation by RclA wild type

and mutants in the absence of Cu^{2+}. The reaction buffer contained 200 μM NADH, 2 μM EcRclA, and 50 μM cytochrome *c*. Superoxide anion production was measured using the amount of reduced cytochrome *c* at 550 nm (line); NADH oxidation was measured at 340 nm (dotted line) over time spectrophotometrically at the same time points. Data are the averages of three independent experiments. Each mutant is shown in a different color.

C. NADH oxidation rate comparison between RclA C43S and wild type with various metal ions. The reaction was performed with 200 μM NADH and 2 μM RclA, and 100 μM of metal ions. A control assay was performed without metal ion. Data are expressed as the mean ± SD of three independent experiments (μmole NADH $\cdot min^{-1} \cdot mg^{-1}$ RclA).

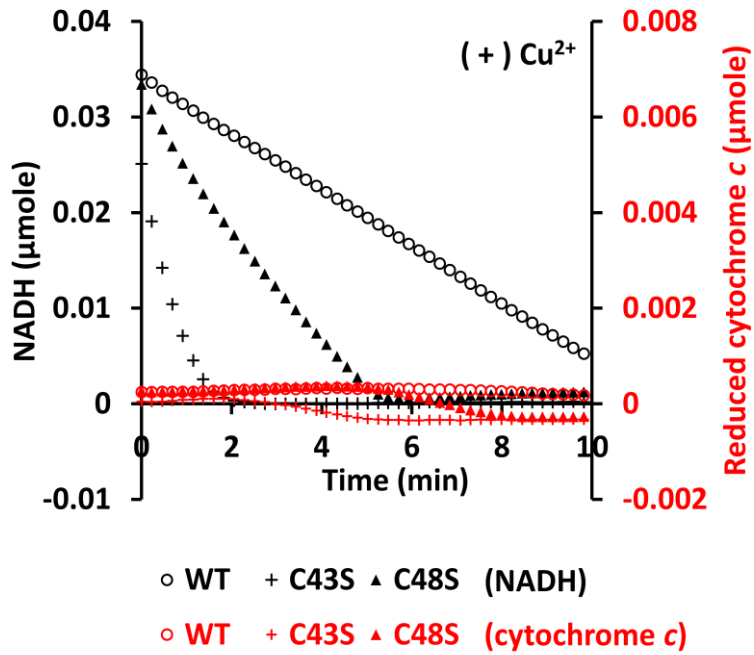

Figure 17. Superoxide anion production during NADH oxidation by RclA wild type and mutants in the presence of Cu^{2+}.

The reaction buffer contained 200 µM NADH, 100 µM $CuCl_2$, 5 µM EcRclA, and 50 µM cytochrome C. Superoxide anion production was measured according to the amount of reduced cytochrome C at 550 nm (line), and NADH oxidation was measured at 340 nm (dotted line) at the same time points. Data are the averages of three independent experiments.

3.10. Structural determination of RclA wild type and RclA C43S in complex with Cu^{2+}

To analyze how Cu^{2+} affects the activity of RclA at the molecular level, crystal structures of EcRclA in complex with Cu^{2+} were determined in the presence of 5 mM $CuCl_2$. To prevent the formation of the disulfide bond in the CXXXXC motif by Cu^{2+}, the complex structure of the EcRclA C43S mutant was further determined (see below). (Fig. 18)

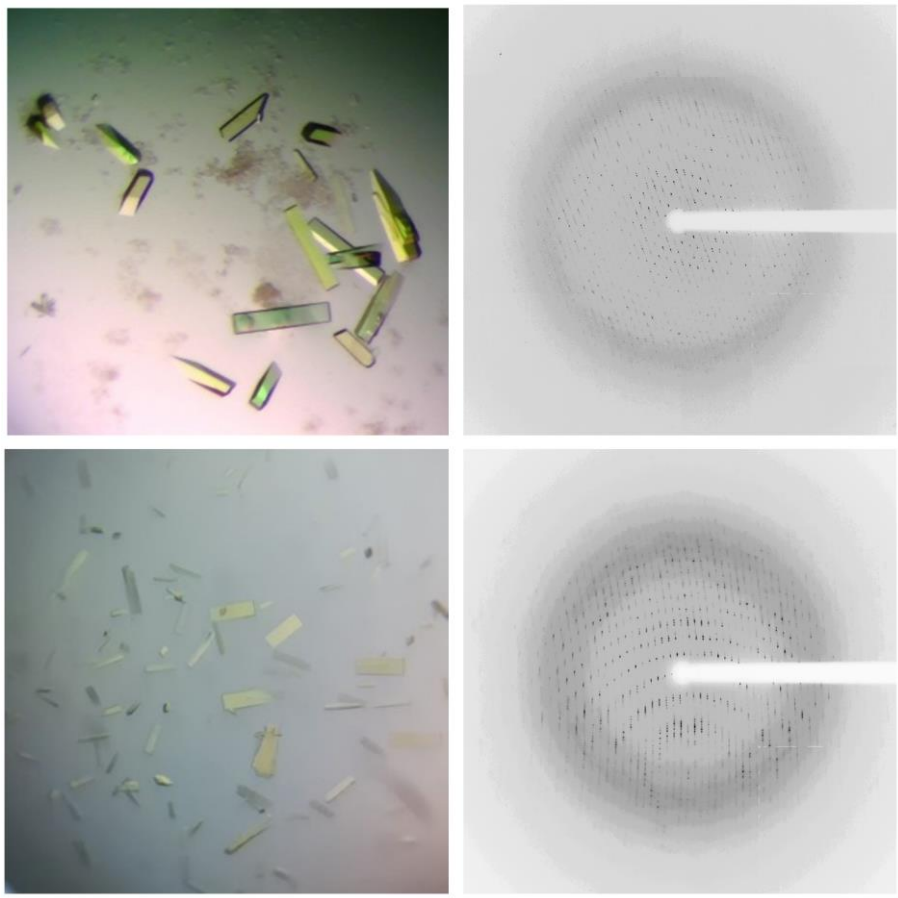

Figure 18. Crystals and X-ray diffraction data of RclA wild type and RclA C43S in complex with Cu^{2+}.

A Crystals of RclA wild type. B, X-ray diffraction data of RclA wild type with 5 mM $CuCl_2$. C, Crystals of RclA C43S. D, X-ray diffraction data of RclA C43S with 5 mM $CuCl_2$.

3.11. Multiple binding of Cu^{2+} to RclA

RclA is a histidine-rich protein containing 16 histidine residues (15 surface-exposed histidine residues and His426 at the active site). Strong Cu^{2+} densities were observed near all of the histidine residues except for His426 in both complex structures, indicating that Cu^{2+} is bound to almost all of the surface-exposed histidine residues of RclA (Fig. 19). However, no apparent structural changes were observed in the complex structures despite the multiple Cu^{2+} binding at the histidine residues (Fig. 20). It is noteworthy that surface-exposed histidine residues are abundant in RclA. Because almost all of the histidine residues of RclA can bind to Cu^{2+} (Fig. 19), RclA could lower the amount of free Cu^{2+} available to participate in the Fenton reaction with HOCl to produce highly toxic hydroxyl radicals.

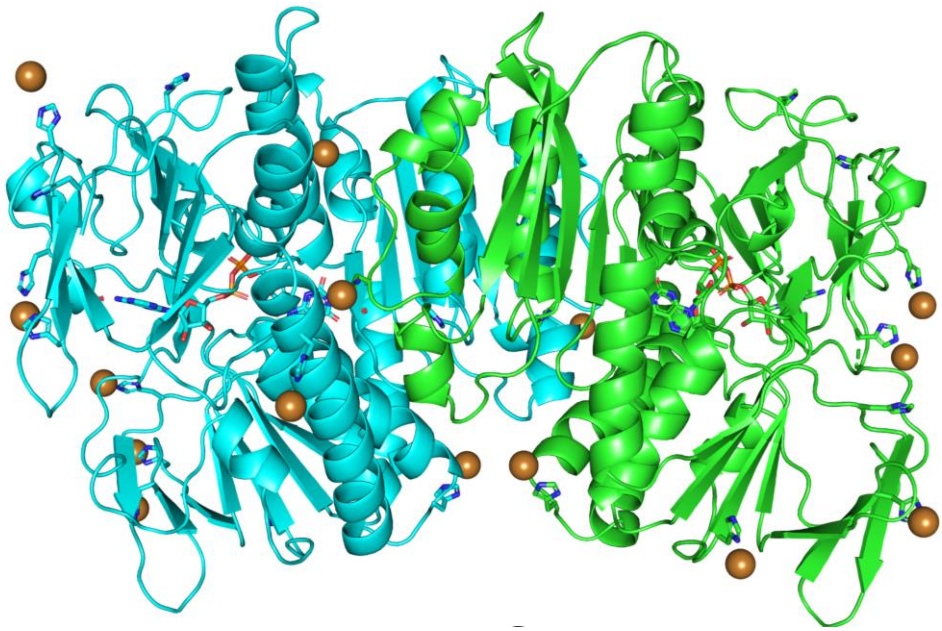

Figure 19. The overall structure of EcRclA wild type in complex with Cu^{2+}

Each subunit is colored differently (cyan, green). Cu^{2+} is shown in the sphere (brown). Histidine residues and the bound FAD are shown in stick representation.

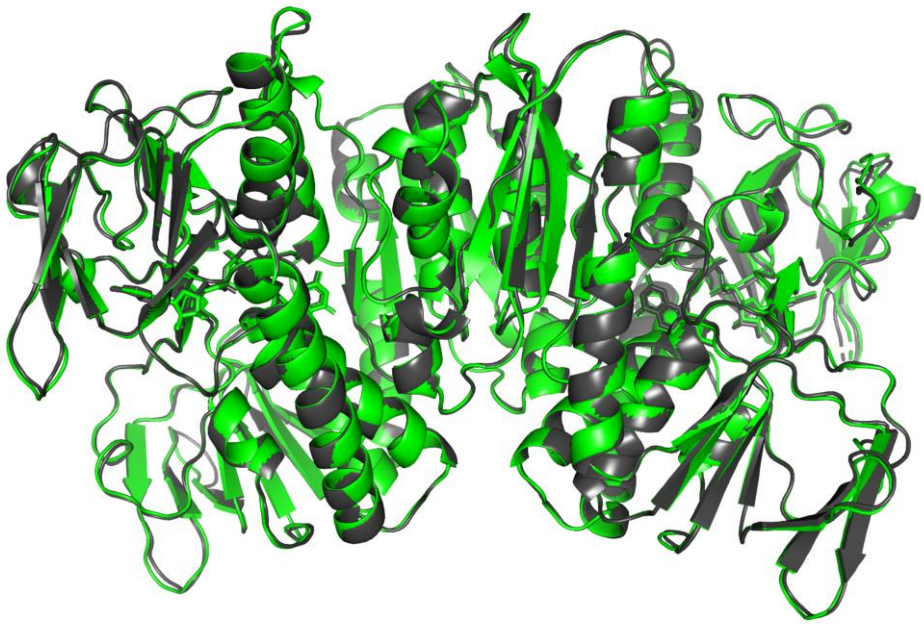

Figure 20. Overall structure comparison of EcRclA wild type with the EcRclA wild type-Cu^{2+} complex.

EcRclA wild type without Cu^{2+} is in grey; EcRclA wild type-Cu^{2+} complex is in green. The RMSD between 776 atoms of each dimer was 0.347

3.12. Cu^{2+} binding at the active site

Strong electron density maps near the cysteine residues at the active site also appeared in Cu^{2+}-soaked crystals of the wild type RclA protein. The maps were suggested as heavy-atom sites in the MR-SAD map containing the anomalous signals from Cu^{2+} by the Phenix program suites. Thus, it is very likely that the strong electron density maps represent the Cu^{2+} binding (Fig. 21A). The Cu^{2+} density maps were in between the sulfur atoms of Cys43 and Cys48 in the CXXXXC motif. Moreover, the densities were not found in the C43S mutant structure, indicating the importance of Cys43 for the binding of Cu^{2+} (Fig. 21B). Combined with the biochemical results with the C43S mutant RclA, the binding between the two cysteine residues is essential in the selectivity to Cu^{2+} over the other metal ions.

Regarding Cys48, the Cys48 residue is located between the Cu^{2+} and the FAD molecule. This structure suggests that Cys48 prevents the direct contact between Cu^{2+} and FAD, and allows the electron flows from FAD to Cu^{2+} via Cys48. This structural arrangement of Cu^{2+}-Cys48-FAD is well supported by our biochemical results that Cys48 contributed to the prevention of basal production of superoxide anion from oxygen.

Two lysine residues (Lys13 and Lys16), which are unique to RclA proteins, were located at the entrance to the active site. To examine the role of the lysine residues, the mutant protein K13A/K16A was produced and compared the K_m and V_{max} values for Cu^{2+} with those of wild type protein.

The mutant protein showed both K_m and V_{max} values decreased by ~1.3 fold with a similar V_{max}/K_m value (Fig. 21C). These biochemical results show that the two lysine residues provide the positively-charged environment to limit the prolonged staying of metal ions, promoting the turn-over of the reaction cycles. Alternatively or concomitantly, this positively-charged environment would attract or capture negatively-charged reaction intermediates for the subsequent reactions.

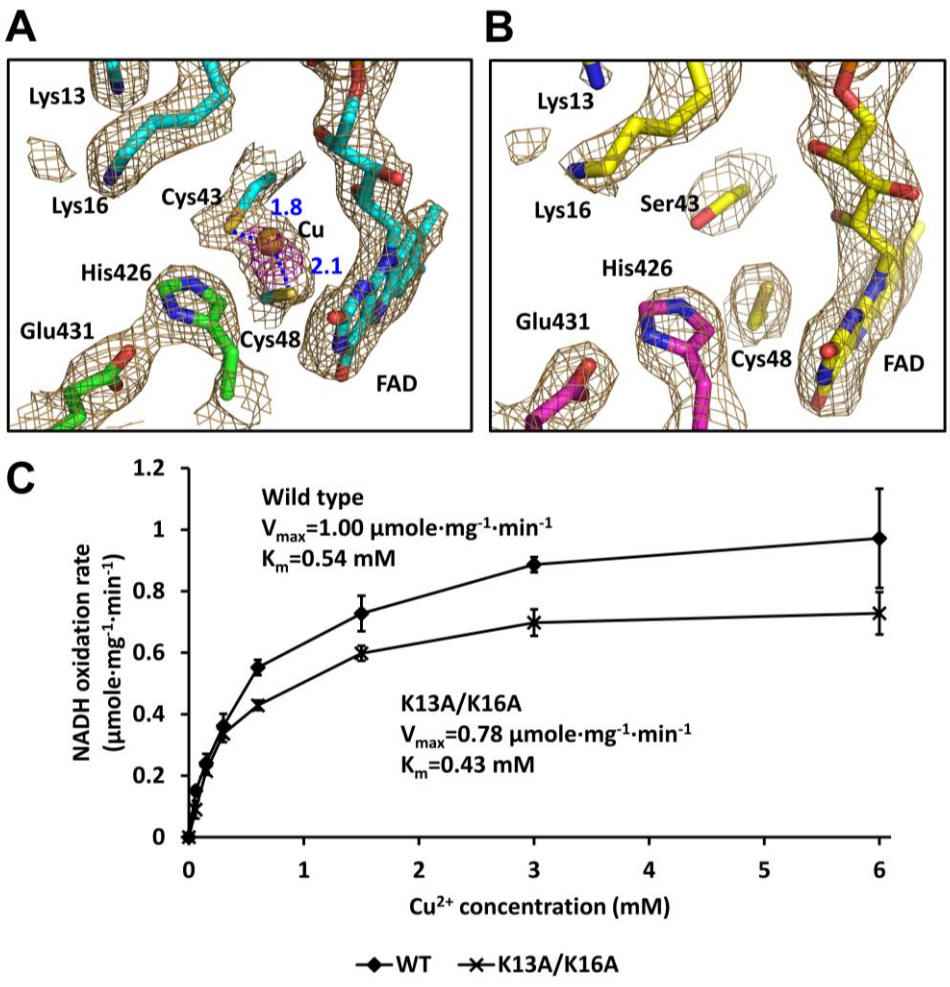

Figure 21. The extra electron density maps at the active site in Cu^{2+}-soaked structures.

A. Binding of Cu^{2+} at the active site of RclA wild type. Each subunit is colored differently (cyan, green). Cu^{2+} is shown in the sphere (brown). The electron density map has been contoured at 1.5 σ (sand). Anomalous difference map of the bound Cu^{2+} has been contoured at 3.0 σ (magenta). Distances are in Å (blue dash)

B. The active site of RclA C43S. Each subunit is colored differently (yellow,

magenta). The electron density map has been contoured at 1.5 σ (sand).

C. The biochemical role of Lys13 and Lys16. Initial velocities of the NADH oxidation by RclA wild type and RclA K13A/K16A were measured for K_m and V_{max}. The reaction was assayed with 2 μM RclA, 200 μM NADH, and 0, 0.6, 0.15, 0.3, 0.6, 1.5, 3, or 6 mM Cu^{2+}. NADH oxidation rates were measured over time spectrophotometrically (n = 3, mean ± SD). V_{max} or K_m value was calculated by fitting the data with a Michaelis-Menten equation using an enzyme kinetics tool of the SigmaPlot Version 14.0 (Systat Software, San Jose, CA)

IV. Discussions

RclA from *E. coli* was reported to increase resistance to HOCl treatment (12). This study using *Salmonella* strains extends the role of RclA in bacterial survival in macrophage phagosomes. To understand the roles of RclA at the molecular level, high-resolution structures of RclA from *E. coli* exhibiting the typical dimeric features of FDR family proteins were elucidated. The structure of EcRclA showed intermingled properties of group I and II FDRs. Although the overall structure of EcRclA was the most similar to the group II FDR MerA, the key motifs in the active site were more closely related to group I FDRs. While this manuscript was in preparation, Derke *et al*. reported that EcRclA is a Cu^{2+} reductase that converts Cu^{2+} into Cu^{+} using the reducing power of NADH to cope with HOCl stress in *Drosophila* (17). Consistently, Cu^{2+} boosted the NADH oxidation activity in a dose-dependent manner, and Cu^{2+} was bound to the active site. Furthermore, the O_2 consumption activity of RclA in the presence of Cu^{2+} was discovered with a limited production of superoxide anion.

Furthermore, the O_2 reduction is required for the Cu^{2+} reduction activity of EcRclA and vice versa, indicating that the NADH oxidation is coupled with the reduction of O_2 dissolved in the buffer. Furthermore, neither the reduced portions of Cu^{2+} nor O_2 was able to account for the released electrons from NADH fully. These findings indicate that the reduction of Cu^{2+}

and O_2 should be simultaneously considered a reaction cycle. Because O_2 is the starting substance to produce HOCl via oxidative burst in immune cells, the reduced level of O_2 in the phagosomes would lower the level of HOCl. To decrease the level of HOCl would be an important role of RclA for bacterial survival in immune cells.

Despite the structural and chemical similarities to MerA mediating a two-electron transfer to a metal ion, a previous study (17) presented evidence for a one-electron transfer to Cu^{2+} producing Cu^{+}. However, it seems odd that Cu^{+} is more active than Cu^{2+} in Fenton-like reactions to produce hydroxyl radicals from HOCl. It is believed that more sophisticated reaction networks with other proteins would be involved.

FDRs are involved in many different chemical reactions using the bound FAD and various electron acceptors, such as disulfide, O_2, or metal ions. In the group I FDR glutathione reductase, electrons from NADPH are transferred to the disulfide of the oxidized glutathione using the CXXXXC motif as the key intermediate. However, a small portion of electrons flows into oxygen to generate superoxide anion or H_2O_2 as a side reaction of FDRs (35). Furthermore, the reduction of glutathione is strongly inhibited by Cu^{2+} (40), indicating that Cu^{2+} is bound at the active site, and thus alters the electron flow in the reaction mechanism as a potential regulator. In the cases of MerA and RclA, the electrons flow into Hg^{2+} and Cu^{2+}, respectively, as the final acceptor, which is the primary reaction of these enzymes. Thus our

findings suggest that binding of metal ions at the active site alters the pathway of electrons from FDRs toward the bound metal ions.

Our structural and mutational studies provide hints on the reaction mechanism of RclA (Fig. 8). This study observed the Cu^{2+} binding in the presumably oxidized FAD-bound structure, presenting the FAD-Cys48-Cu^{2+}-Cys43 network as the critical electron flow route. The reaction would be triggered when the electrons are provided to FAD by NADH in the presence of O_2. The electrons released from $FADH_2$ are first transferred to Cys48 and then transferred to the bound Cu^{2+} with the Cys43. This Cys48-mediated electron transfer to Cu^{2+} is consistent with the result that the Cu^{2+} dependency in NADH oxidation disappeared with increased levels of superoxide anion production in the C48S mutant. It is proposed that the Cys48 prevents the direct single electron transfer from $FADH_2$ to O_2 by absorbing electron from $FADH_2$ leading to suppression of superoxide anion production, and transfer the received electrons to Cu^{2+}.

The Cu^{2+}-bound structure, together with the results of the C43S mutation, demonstrated that Cys43 is directly involved in the binding of Cu^{2+}. This C-terminal cysteine residue (Cys43) in the CXXXXC motif would affect the specificity of various metal ions, as the C43S mutant showed different NADH oxidation rates with metal ions compared to the wild type. Since the sulfur atom of Cys43 and the imidazole ring of His426 are within a distance to make a hydrogen bond, the His426-Glu431 pair in the HXXXXE motif

would deprotonate Cys43, promoting binding with the Cu^{2+}. Furthermore, the His-Glu pair could also transfer protons to proton or electron acceptors during the catalysis. To reduce oxygen, the electron transfer should accompany the proton transfer. Thus this proton transfer mediated by this HXXXXE motif would also be important for the catalysis.

Because of the complexity of the reactions, multiple rounds might be required to complete the reaction. Regarding the two lysine residues at the active site, the negatively-charged reaction intermediates such as superoxide anion might be captured by the lysine residues. The oxygen might eventually be transformed into water molecules upon this Cu^{2+}-mediated reaction through the multiple rounds of electron and proton transfers. However, further studies are required to elucidate the electron transfer reactions.

Reactions of RclA, the Cu^{+}-specific CopA in the inner membrane, the Cu^{+} oxidase CueO in the periplasm, and the Cu^{2+}- specific CusABC efflux pump can be combined in the cytoplasm. (Fig. 23). RclA converts Cu^{2+} into Cu^{+} with the consumption of O_2 by NADH. The reduced Cu^{+} can be exported by Cu^{+} efflux pump (41) or transported into the periplasm by Cu^{+} specific copper-exporting P-type ATPase CopA (42). The Cu^{+} oxidase CueO oxidizes Cu^{+} to Cu^{2+} by using O_2 in the periplasm (43), or the transported Cu^{+} can go out of the cell by the Cus system from the periplasm (41). Thus the net reaction of the four proteins is that Cu^{2+} is transported from the cytoplasm to the periplasm or out of the cell, and the oxygen in the cytosol and the

periplasm are depleted. Since Cu^{2+} in the cytoplasm could mediate the Fenton-like reaction with HOCl, the lowering level of Cu^{2+} would be beneficial for bacterial survival. Furthermore, the O_2 consumption activity of RclA in the presence of Cu^{2+} with a limited production of superoxide anion is important. Molecular oxygen is the starting substance to produce HOCl via oxidative bursts in the immune cells. Thus the reduced level of oxygen in the phagosomes capturing the bacteria would lower the level of HOCl, which would be an important role of RclA for the bacteria to survive in the immune cells.

The HOCl resistance mechanism of RclA gave insights into controlling food-borne pathogens with HOCl-based sanitizers in food processing. The dose of HOCl treatment in food sanitizing needs to be controlled, as a high concentration of HOCl can damage the sanitized food and there can be residual chlorine and side products of HOCl. The HOCl treatment with the RclA inactivation by its inhibitor can lower the dose of HOCl treatment with increased antimicrobial effect.

In conclusion, a high-resolution structure of RclA was used to investigate its biochemical roles and functions in the HOCl resistance of bacteria. Although further study is required to elucidate the molecular mechanism, our study provides a molecular basis for how bacteria can cope with our immune system, which may help in the creation of strategies to control pathogenic bacteria.

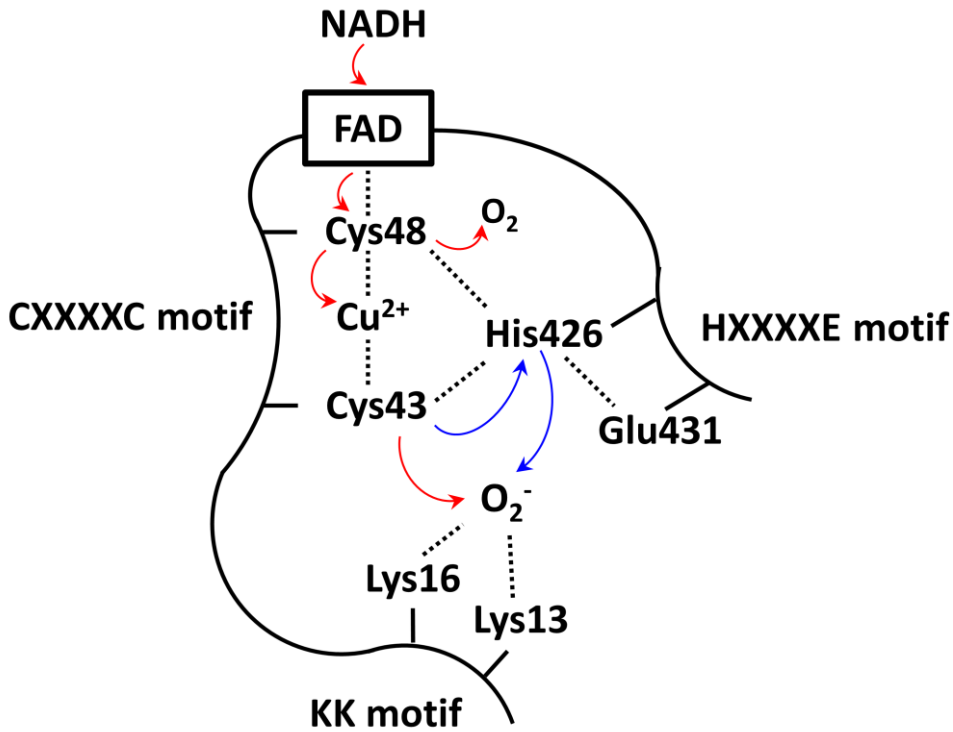

Figure 22. A proposed reaction order of O_2 and Cu^{2+} reduction by EcRclA.

Red arrows represent electron flow. Blue arrows represent proton flow. Residues, substrates, and products of EcRclA are presented in black. The bound FAD in EcRclA is presented in a black box. Interactions between two amino acid residues or between an amino acid residue and Cu^{2+} ion are shown as dashed lines.

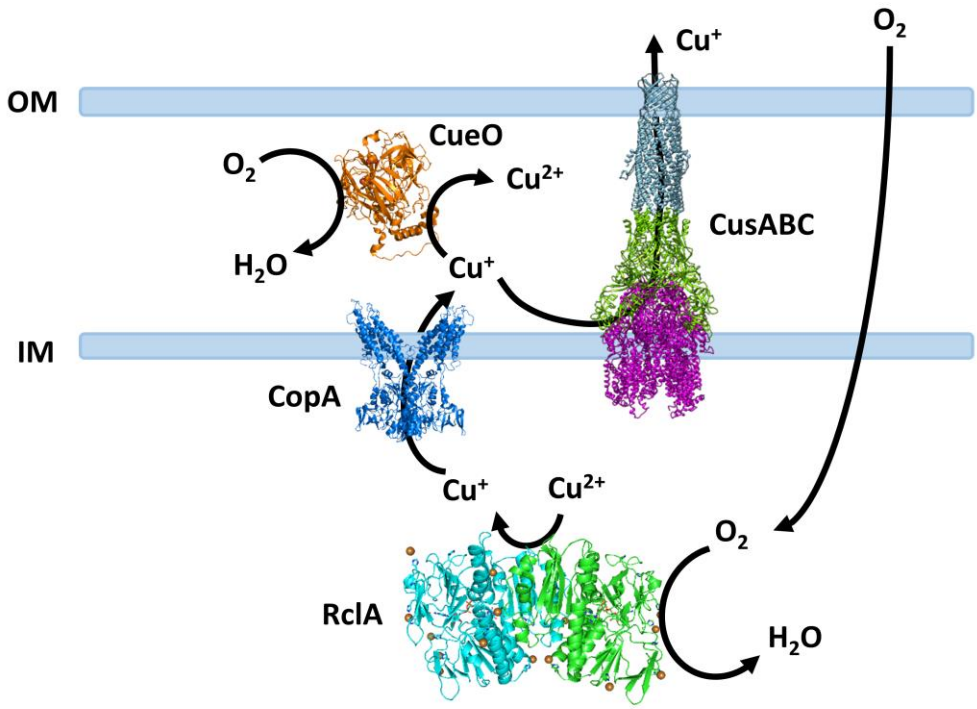

Figure 23. The proposed biological role of RclA in the bacterial cell

OM is the bacterial outer membrane, IM is the bacterial inner membrane, CopA is a bacterial p-type ATPase copper transporter (PDB code: 3j08), CusABC is a modeled structure of Cu^{2+}- specific efflux pump from (41), CueO is a multicopper oxidase from *E. coli* (PDB code: 3OD3).

V. References

1. Leyer, G. J., and Johnson, E. A. (1997) Acid adaptation sensitizes Salmonella typhimurium to hypochlorous acid. *Appl. Environ. Microbiol.* 63, 461-467
2. Jaquette, C. B., Beuchat, L. R., and Mahon, B. E. (1996) Efficacy of chlorine and heat treatment in killing Salmonella stanley inoculated onto alfalfa seeds and growth and survival of the pathogen during sprouting and storage. *Appl. Environ. Microbiol.* 62, 2212-2215
3. Kotula, K. L., Kotula, A. W., Rose, B. E., Pierson, C. J., and Camp, M. (1997) Reduction of aqueous chlorine by organic material. *Journal of Food Protection* 60, 276-282
4. Weiss, S. J., and LoBuglio, A. F. (1982) Phagocyte-generated oxygen metabolites and cellular injury. *Lab Invest* 47, 5-18
5. Ha, E. M., Oh, C. T., Bae, Y. S., and Lee, W. J. (2005) A direct role for dual oxidase in Drosophila gut immunity. *Science* 310, 847-850
6. Winterbourn, C. C., and Kettle, A. J. (2013) Redox reactions and microbial killing in the neutrophil phagosome. *Antioxid Redox Signal* 18, 642-660
7. Hampton, M. B., Kettle, A. J., and Winterbourn, C. C. (1998) Inside the neutrophil phagosome: oxidants, myeloperoxidase, and bacterial killing. *Blood* 92, 3007-3017

8. Hawkins, C. L., Pattison, D. I., and Davies, M. J. (2003) Hypochlorite-induced oxidation of amino acids, peptides and proteins. *Amino Acids* 25, 259-274

9. Davies, M. J. (2005) The oxidative environment and protein damage. *Biochim Biophys Acta* 1703, 93-109

10. Gray, M. J., Wholey, W. Y., and Jakob, U. (2013) Bacterial responses to reactive chlorine species. *Annu Rev Microbiol* 67, 141-160

11. Folkes, L. K., Candeias, L. P., and Wardman, P. (1995) Kinetics and mechanisms of hypochlorous acid reactions. *Arch Biochem Biophys* 323, 120-126

12. Parker, B. W., Schwessinger, E. A., Jakob, U., and Gray, M. J. (2013) The RclR protein is a reactive chlorine-specific transcription factor in Escherichia coli. *The Journal of biological chemistry* 288, 32574-32584

13. Gebendorfer, K. M., Drazic, A., Le, Y., Gundlach, J., Bepperling, A., Kastenmüller, A., Ganzinger, K. A., Braun, N., Franzmann, T. M., and Winter, J. (2012) Identification of a hypochlorite-specific transcription factor from Escherichia coli. *Journal of Biological Chemistry* 287, 6892-6903

14. Gray, M. J., Wholey, W.-Y., Parker, B. W., Kim, M., and Jakob, U. (2013) NemR is a bleach-sensing transcription factor. *Journal of Biological Chemistry* 288, 13789-13798

15. Jo, I., Kim, D., No, T., Hong, S., Ahn, J., Ryu, S., and Ha, N.-C. (2019) Structural basis for HOCl recognition and regulation mechanisms of HypT, a hypochlorite-specific transcriptional regulator. *Proceedings of the National Academy of Sciences* 116, 3740-3745

16. Martin, R. G., and Rosner, J. L. (2001) The AraC transcriptional activators. *Current opinion in microbiology* 4, 132-137

17. Derke, R. M., Barron, A. J., Chaple, I. F., Lapi, S. E., Broderick, N. A., and Gray, M. J. (2019) RclA is a thermostable copper (II) reductase required for reactive chlorine resistance and host colonization in Escherichia coli. *bioRxiv*, 690669

18. Argyrou, A., and Blanchard, J. S. (2004) Flavoprotein disulfide reductases: advances in chemistry and function. *Progress in nucleic acid research and molecular biology* 78, 89-142

19. Novoradovsky, A., Zhang, V., Ghosh, M., Hogrefe, H., Sorge, J. A., and Gaasterland, T. (2005) Computational principles of primer design for site directed mutagenesis. in *Technical Proceedings of 2005 NSTI Nanotechnology Conference and Trade Show*

20. Park, S.-Y., Ha, S.-C., and Kim, Y.-G. (2017) The protein crystallography beamlines at the pohang light source II. *Biodesign* 5, 30-34

21. Otwinowski, Z., and Minor, W. (1997) Processing of X-ray diffraction data collected in oscillation mode. in *Methods in enzymology*, Elsevier.

pp 307-326

22. Winn, M. D., Ballard, C. C., Cowtan, K. D., Dodson, E. J., Emsley, P., Evans, P. R., Keegan, R. M., Krissinel, E. B., Leslie, A. G., and McCoy, A. (2011) Overview of the CCP4 suite and current developments. *Acta Crystallographica Section D: Biological Crystallography* 67, 235-242

23. Shin, W.-H., Lee, G. R., Heo, L., Lee, H., and Seok, C. (2014) Prediction of protein structure and interaction by GALAXY protein modeling programs. *Bio Design* 2, 1-11

24. Ko, J., Park, H., Heo, L., and Seok, C. (2012) GalaxyWEB server for protein structure prediction and refinement. *Nucleic acids research* 40, W294-W297

25. Emsley, P., and Cowtan, K. (2004) Coot: model-building tools for molecular graphics. *Acta Crystallographica Section D: Biological Crystallography* 60, 2126-2132

26. Afonine, P. V., Mustyakimov, M., Grosse-Kunstleve, R. W., Moriarty, N. W., Langan, P., and Adams, P. D. (2010) Joint X-ray and neutron refinement with phenix. refine. *Acta Crystallographica Section D: Biological Crystallography* 66, 1153-1163

27. Banzi, M., and Shiloh, M. (2014) *Getting started with Arduino: the open source electronics prototyping platform*, Maker Media, Inc.

28. Di Tommaso, P., Moretti, S., Xenarios, I., Orobitg, M., Montanyola,

A., Chang, J.-M., Taly, J.-F., and Notredame, C. (2011) T-Coffee: a web server for the multiple sequence alignment of protein and RNA sequences using structural information and homology extension. *Nucleic Acids Research* 39, W13-W17

29. Robert, X., and Gouet, P. (2014) Deciphering key features in protein structures with the new ENDscript server. *Nucleic Acids Research* 42, W320-W324

30. Holm, L. (2019) Benchmarking Fold Detection by DaliLite v. 5. *Bioinformatics*

31. Rennex, D., Pickett, M., and Bradley, M. (1994) In vivo and in vitro effects of mutagenesis of active site tyrosine residues of mercuric reductase. *FEBS letters* 355, 220-222

32. Lian, P., Guo, H.-B., Riccardi, D., Dong, A., Parks, J. M., Xu, Q., Pai, E. F., Miller, S. M., Wei, D.-Q., and Smith, J. C. (2014) X-ray structure of a Hg2+ complex of mercuric reductase (MerA) and quantum mechanical/molecular mechanical study of Hg2+ transfer between the C-terminal and buried catalytic site cysteine pairs. *Biochemistry* 53, 7211-7222

33. Angiulli, G., Lantella, A., Forte, E., Angelucci, F., Colotti, G., Ilari, A., and Malatesta, F. (2015) Leishmania infantum trypanothione reductase is a promiscuous enzyme carrying an NADPH: O2 oxidoreductase activity shared by glutathione reductase. *Biochimica*

et Biophysica Acta (BBA)-General Subjects 1850, 1891-1897

34. Geueke, B., Riebel, B., and Hummel, W. (2003) NADH oxidase from Lactobacillus brevis: a new catalyst for the regeneration of NAD. *Enzyme and Microbial Technology* 32, 205-211

35. Imlay, J. A. (2013) The molecular mechanisms and physiological consequences of oxidative stress: lessons from a model bacterium. *Nature Reviews Microbiology* 11, 443

36. Massey, V., Strickland, S., Mayhew, S. G., Howell, L. G., Engel, P., Matthews, R. G., Schuman, M., and Sullivan, P. (1969) The production of superoxide anion radicals in the reaction of reduced flavins and flavoproteins with molecular oxygen. *Biochemical and biophysical research communications* 36, 891-897

37. Liochev, S. I., and Fridovich, I. (1992) Superoxide generated by glutathione reductase initiates a vanadate-dependent free radical chain oxidation of NADH. *Arch Biochem Biophys* 294, 403-406

38. Ledwidge, R., Patel, B., Dong, A., Fiedler, D., Falkowski, M., Zelikova, J., Summers, A. O., Pai, E. F., and Miller, S. M. (2005) NmerA, the metal binding domain of mercuric ion reductase, removes Hg2+ from proteins, delivers it to the catalytic core, and protects cells under glutathione-depleted conditions. *Biochemistry* 44, 11402-11416

39. Ray, S., Gachhui, R., Pahan, K., Chaudhury, J., and Mandal, A. (1989) Detoxification of mercury and organomercurials by nitrogen-fixing

soil bacteria. *Journal of Biosciences* 14, 173-182

40. Murakami, K., Tsubouchi, R., Fukayama, M., and Yoshino, M. (2014) Copper-dependent inhibition and oxidative inactivation with affinity cleavage of yeast glutathione reductase. *Biometals* 27, 551-558

41. Jo, I., Kim, J.-S., Xu, Y., Hyun, J., Lee, K., and Ha, N.-C. (2019) Recent paradigm shift in the assembly of bacterial tripartite efflux pumps and the type I secretion system. *Journal of Microbiology* 57, 185-194

42. Rensing, C., Fan, B., Sharma, R., Mitra, B., and Rosen, B. P. (2000) CopA: an Escherichia coli Cu (I)-translocating P-type ATPase. *Proceedings of the National Academy of Sciences* 97, 652-656

43. Singh, S. K., Roberts, S. A., McDevitt, S. F., Weichsel, A., Wildner, G. F., Grass, G. B., Rensing, C., and Montfort, W. R. (2011) Crystal structures of multicopper oxidase cueO bound to copper (I) and silver (I) functional role of a methionine-rich sequence. *Journal of Biological Chemistry* 286, 37849-37857

VI. 국문 초록

차아염소산은 강력한 살균제로, 예로부터 병원균을 제어하기 위해 다양한 식품의 살균에 이용되어 왔다. 차아염소산은 본래 진학 생물의 면역 시스템에서 산화적 폭발을 통해 미생물을 죽이기 위하여 산소로부터 생산된다. 또한 호중구와 대식세포의 식포 안에서는 구리를 유입시켜 차아염소산의 독성을 증폭시킨다. 그러나 대장균과 살모넬라균에서는 차아염소산 스트레스에 방어하기 위해 전사 인자 RclR이 차아염소산 스트레스를 인식하여 RclA, RclB, RclC 단백질의 발현을 유도한다. 현재 Rcl 단백질들의 구조와 생화학적인 역할은 명확히 알려져 있지 않다. 본 연구에서는 플라빈 단백질 이황화물 환원 효소인 RclA의 분자적인 기작을 이해하기 위하여 대장균 RclA의 결정 구조를 규명하였다. 동종이량체를 이루는 RclA는 보조 인자인 FAD의 플라빈 고리 근처에 두 개의 보존된 시스테인 잔기들을 가지고 있어 전형적인 플라빈단백질 이황화물 환원 효소와 유사했다. RclA에 의한 NADH의 산화를 구리 이가 양이온이 환원되며 가속화하면서, 용액 안의 산소 농도를 낮추는 것을 관찰하였다. 보존된 시스테인 잔기들의 돌연변이는 구리 이가 양이온에 대한 특이성을 낮추거나, 구리 이가 양이온이

없는 조건에서 초과산화물 음이온 라디칼의 생성을 야생형에 비해 상당히 증가시켰다. RclA에 의해 낮아진 산소 농도는 면역세포의 식포 내에서 차아염소산 생성 저해에 기여하며, 환원된 구리 일가 양이온은 세포 밖으로 배출되어 세포질에서 차아염소산과의 라디칼 생성 반응이 저해될 것이다. 본 연구는 세균이 인체 면역 시스템 내의 차아염소산 스트레스에서 살아남는 분자적 기전을 제시하였다. RclA의 차아염소산 저항 기전은 또한 차아염소산을 이용한 식품 살균의 새로운 가능성을 제시한다. 병원균의 RclA를 저해하면 보다 저농도의 차아염소산을 사용하면서도 살균 효과를 증대시킬 수 있을 것이다.

주요어: 차아염소산, 플라빈단백질 이황화결합 환원효소, 구리 이온, 산소, 결정 구조

학번: 2018-26723